

Oscillating Cantilever Magnetometry in High Magnetic Fields

High Field Magnet Laboratory

Radboud University



Andrew Ammerlaan

Supervisor: Prof. Dr. Uli Zeitler

October 21, 2020

Abstract

In this thesis we have extended HFML's torque magnetometry setup to an oscillating cantilever magnetometry setup. We have done this by glueing a coil onto the cantilever. By sending a sinusoidal current through this coil the cantilever is forced to oscillate. If a sample is also glued onto the cantilever, its magnetization will effect these oscillations when the setup is inside a magnetic field. When the change in these oscillations is measured, the magnetization of the sample can be determined. Our setup is characterized, and using a capacitance bridge the change in amplitude of the oscillations caused by an InSb sample is measured as a function of magnetic field. We find that in principle our setup and method works. However, our results show us that we cannot resolve the effect of the sample using this method, this finding is consistent with simulations of our setup. Therefore, more work still needs to be done before actual measurements can be done with this setup. Possible extensions of our experiments that might prove promising consists of measuring either the phase or resonant frequency instead of the amplitude.

Contents

1	Introduction	3
2	Magnetism and Quantum Oscillations	4
2.1	Magnetization	4
2.2	Quantum Oscillations in a 3D Quasi-Free Electron Gas	4
2.2.1	Shunikov-de-Haas Oscillations	6
2.2.2	Simulating de-Haas-van-Alphen Oscillations	7
3	Torque Magnetometry	10
3.1	Capacitive Measurement of Torque	11
3.2	Other Ways to Measure Torque	14
3.3	Setup at HFML	14
3.4	Setup Characterization	15
3.4.1	Field Profile	15
3.4.2	Linearity of the Cantilever	19
3.4.3	Smaller coils	21
3.5	De-Haas-van-Alphen effect	25
4	Oscillating Cantilever Magnetometry	27
4.1	Simulating Cantilever Magnetometry	28
4.1.1	Amplitude	28
4.1.2	Phase	31
4.1.3	Resonant Frequency	32
5	Conclusion and Discussion	34
5.1	Suggestions for further research	34
6	Acknowledgements and References	36
A	Integral Solution	37
B	Differential Equation Solution	40
C	Cantilever Specifications and Oscillation Data	43

1 Introduction

Torque magnetometry is a common method for determining the magnetization of a sample. The sample exerts a torque on a cantilever depending on the sample's magnetization, this torque causes the cantilever to bend and this bending can be measured in the a change of the capacitance between the cantilever and a base plate. By extending this setup to oscillating cantilever magnetometry we in effect turn a DC measurement into an AC measurement. An AC measurement is inherently more accurate because we can measure and average over multiple periods of the oscillation, thereby increasing the sampling rate and thus decreasing the errors. This extension of the setup is in principle simple, we glue a coil onto the cantilever and send a sinusoidal current through this coil. The oscillating magnetic moment of the coil will force the cantilever to oscillate in a magnetic field. These physical oscillations of the cantilever express themselves in the resulting oscillations in the capacitance between the cantilever and the base plate.

We will start this thesis by describing the theory on magnetization and quantum oscillations in Section 2, here we will present a measurement of these quantum oscillations in the conductivity: the Shubnikov-de-Haas effect. In Section 3 we will continue with the operating principle behind the torque magnetometer, and describe and characterize our extended setup. We will try to measure quantum oscillations in the magnetization of a sample of Indium Antimonide. Subsequently we simulate our setup in Section 4. And finally we summarize our conclusions and give suggestions for further research in Section 5.

2 Magnetism and Quantum Oscillations

2.1 Magnetization

Electrons in any material will react to an external magnetic field applied to this material, it will do this paramagnetically, diamagnetically, (anti)ferromagnetically, and/or (anti)ferrimagnetically. Here we will focus on paramagnetism and diamagnetism, as these are the only relevant effects for our experiments.

Paramagnetic contributions are caused by the **alignment of magnetic moments** in the material. This causes an internal magnetic field in the material which is parallel to the external field (positive magnetization). Paramagnetic effects are only observed in materials where the atoms/molecules have net magnetic moments, such as materials with an unequal number of spin up and down electrons in the Brillouin zone. Furthermore, paramagnetic materials always saturate at sufficiently large magnetic fields. This is because at some point all magnetic moments in the material are already fully aligned to the magnetic field, and applying more magnetic field no longer has any effect.

Diamagnetism on the other hand is a quantum mechanical effect which can intuitively be described as being caused by the **Lorentz force on the electrons**, this force pushes the electrons into circular orbitals around the magnetic field lines creating an internal magnetic field antiparallel to the external field (negative magnetization). In effect this antiparallel field repels some of the applied field from the material's interior. All materials are diamagnetic to some extent. However, electrons are constrained into specific orbitals by the atom it is orbiting and by the Pauli principle. This causes diamagnetic contributions in general to be much smaller than they would be for a perfect diamagnetic such as a superconductor which completely expels magnetic fields from its interior (Meissner effect). Materials where paramagnetic effects are stronger than diamagnetic effects are called paramagnetic materials. Materials that are not paramagnetic (i.e. the atoms do not have a net magnetic moment) or where the diamagnetic contributions are stronger are called diamagnetic materials.[7].

2.2 Quantum Oscillations in a 3D Quasi-Free Electron Gas

When applying a magnetic field to free charged particles, the Lorentz force will push these charged particles into a specific circular orbit depending on their charge, kinetic energy and the strength of the magnetic field. The same is true for electrons bound to a nucleus. Due to quantum mechanical nature of these particles only orbitals with certain radius are allowed (the phase must match after a rotation of 2π , otherwise destructive interference occurs). These orbitals are called Landau Levels, and the energy of an electron in the n^{th} Landau Level can be found by solving the time-independent Schrödinger equation for a charged particle in a magnetic field: [10, 11]

$$E\psi = \frac{1}{2m_e} \left(-i\hbar\vec{\nabla} - e\vec{A} \right)^2 \psi \quad (2.1)$$

$$E_n = \hbar\omega_c \left(n + \frac{1}{2} \right) + \frac{\hbar^2 k_B^2}{2m_e^*} \quad (2.2)$$

Where k_B is the magnitude of the k vector in the direction of the magnetic field B , m_e^* is the effective mass of the electron, and ω_c is the cyclotron frequency which is given by:

$$\omega_c = \frac{eB}{m_e^*} \quad (2.3)$$

Here e is the electron charge, and m_e^* is the effective cyclotron mass. For parabolic band structures

the effective cyclotron mass is equal to the regular effective mass. Neglecting, for the moment being, temperature effects, only Landau Levels whose energy is lower than the Fermi energy E_f will be occupied. Furthermore, Equations 2.2 and 2.3 show us that the energy of each Landau Level increases when the strength of the applied magnetic field is increased. Therefore, as we increase the magnetic field, eventually the energy of Landau Level n will exceed the Fermi energy. This causes the electrons in Landau level n to leave this Landau level, and redistribute themselves over the Landau levels $n - 1, n - 2, \dots, 0$ whose energy still is below the Fermi energy. Therefore, as the magnetic field increases, we have a periodic reorganisation of electrons over the Landau levels every time a level's energy starts exceeding the Fermi energy. We can calculate the frequency of this periodic reorganisation by equating the energy of Landau level n at magnetic field B with the energy of Landau level $n - 1$ at magnetic field B' , for simplicity we choose this energy to be the Fermi energy:

$$E_f = \hbar \frac{eB}{m_c^*} \left(n + \frac{1}{2} \right)$$

$$E_f = \hbar \frac{eB'}{m_c^*} \left(n - 1 + \frac{1}{2} \right)$$

These equations merely state that the energy of Landau level n reaches the Fermi energy at a magnetic field strength of B , and similarly that the energy of level $n - 1$ reaches the Fermi energy at B' . Next we rewrite the first equation and substitute it into the second:

$$E_f \frac{m_c^*}{\hbar e B} = \left(n + \frac{1}{2} \right)$$

$$E_f = \hbar \frac{eB'}{m_c^*} \left(E_f \frac{m_c^*}{\hbar e B} - 1 \right)$$

Working out the brackets gives:

$$E_f = E_f \frac{B'}{B} - \hbar \frac{eB'}{m_c^*}$$

Dividing the equation by B' and bringing all terms with B and B' to the left gives:

$$\frac{E_f}{B'} - \frac{E_f}{B} = -\hbar \frac{e}{m_c^*}$$

Now dividing by $-E_f$ gives us:

$$\frac{1}{B} - \frac{1}{B'} = \Delta \left(\frac{1}{B} \right) = \frac{\hbar e}{E_f m_c^*} \quad (2.4)$$

Equation 2.4 shows us that this reorganisation of electrons over the Landau levels is periodic with $1/B$.

Since the properties of a material are strongly dependent on the configuration of the electrons in the material, one can imagine that as the electrons reorganise themselves over lower Landau levels certain properties of the material will change as well. Due to the $1/B$ periodic nature of these reorganisations, these changes in the properties of the material will also be $1/B$ periodic. These oscillations are called Quantum Oscillations.

Two important properties which exhibit Quantum Oscillations are the magnetization and the conductivity, the oscillating effect in these properties is called the de-Haas-van-Alphen[11] effect and the Shubnikov-de-Haas[10] effect respectively.

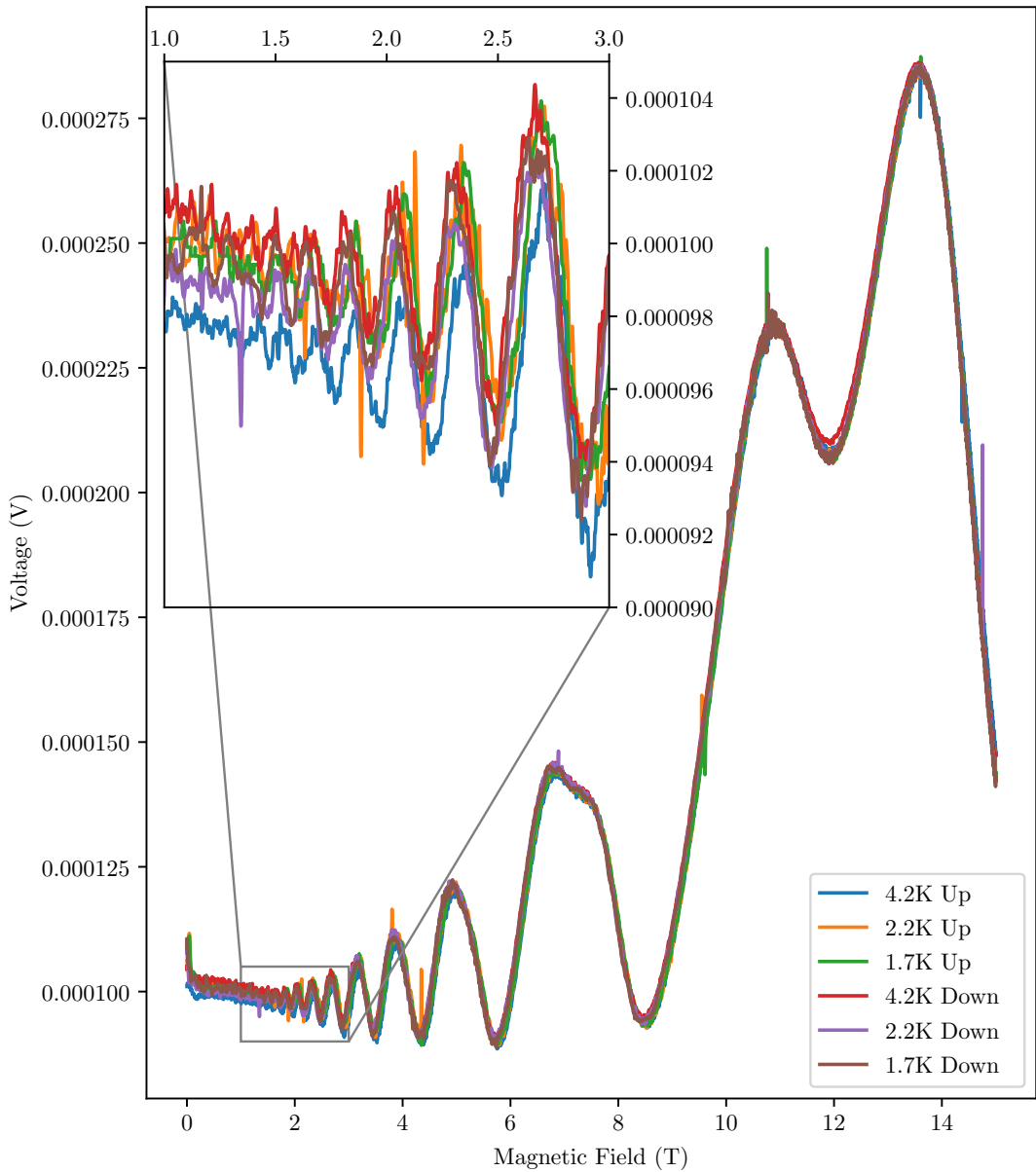
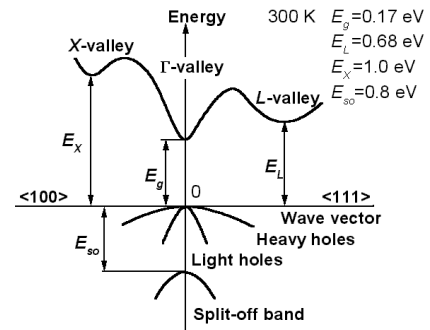


Figure 2.2: Transport measurement of InSb.

2.2.1 Shunikov-de-Haas Oscillations

Indium Antimonide (InSb) is a type III-V semiconductor with a very small direct bandgap of 0.23 eV. The maximum of the valance band, and the minimum of the conduction band both occur at the Γ -point, that is the centre of the Brillouin zone. In addition, the bands are highly parabolic around the Γ -point, as shown in Figure 2.1, and the Fermi surface is well approximated by a sphere[9]. When InSb is not doped the Fermi energy lies in the bandgap. By n-doping the material, electrons are added to the system and the Fermi energy will be in the conduction band. Due to the high parabolicity of the conduction band these electrons behave almost as if they were free electrons. This property makes InSb an ideal material to

Figure 2.1: Band structure of Indium Antimonide around the Γ -point

study quantum oscillations, and also make these oscillations in the properties of InSb relatively easy to simulate.

We have measured the Shunikov-de-Haas oscillations in InSb, the results are shown in Figure 2.2. We can see clear quantum oscillations in the conductivity here down to about 1.5 T, for the higher temperatures we see that the oscillations fade out slightly faster. For fields above 7 T we start to see spin splitting, the conductivity maxima for spin up and down electrons are separated and the higher the field gets the bigger the gap between these two maxima.

Having measured the quantum oscillations in the conductivity, we aim to measure these same oscillations in the magnetization of InSb, that is the de-Haas-van-Alphen oscillations. We have extended our torque magnetometry setup to include a coil and thus allowing driven oscillations of the cantilever, thus we now have an oscillating cantilever magnetometry setup. We will first characterize our extended setup before we will attempt to measure the de-Haas-van-Alphen oscillations. Due to the Covid-19 pandemic experimental time was limited, and a major part of this thesis therefore consist of simulations. In the next section we will see the first of such simulations, there we simulate the de-Haas-van-Alphen effect in InSb.

2.2.2 Simulating de-Haas-van-Alphen Oscillations

The aim of this simulation is twofold. First we aim to get a better idea of what to expect of the de-Haas-van-Alphen oscillations in terms of amplitude and frequency. Second we need this simulation for our further simulations later on.

The magnetic moment m of a 3D electron system of volume V in a magnetic field B (de-Haas-van-Alphen effect) is given by: [8, 11]

$$m = -0.2602VFT \sum_{R=1}^{\infty} \sqrt{\frac{2\pi R}{A''B}} \frac{\cos\left(\frac{\pi}{2}gR\frac{m_c^*}{m_0}\right)e^{-\left(\frac{R\pi}{\mu B}\right)}}{\sinh\left(14.7R\frac{m_c^*T}{m_0B}\right)} \cos\left(\frac{2\pi RF}{B} - \frac{\pi}{4} - 2\pi pR\right) \quad (2.5)$$

Here μ is the electron mobility, m_0 is the free electron rest mass, p is a phase factor (for a parabolic band $p=0.5$ [8]), A is the extremal area of the cross-section of the Fermi surface, and A'' indicates the second order derivative to k_f of this area. It is usually not necessary to include a lot of higher order (larger R) terms, as the higher terms become exponentially smaller. F is the frequency of the oscillations which is given by the inverse of Equation 2.4:

$$F = E_f \frac{m_c^*}{\hbar e} = \frac{\hbar^2 k_f^2}{2m_e^*} \frac{m_c^*}{\hbar e} = \frac{\hbar A}{2\pi e} \quad (2.6)$$

Where in the second step we have assumed a parabolic dispersion relation ($E = \frac{\hbar^2 k^2}{2m_e^*}$, $p = 0.5$, $m_c^* = m_e^*$) and a spherical Fermi surface ($A = \pi k_f^2$, $2\frac{4}{3}\pi k_f^3 = N \left(\frac{2\pi}{L}\right)^3 \Rightarrow k_f = \sqrt[3]{3\pi^2 n}$). Furthermore, for a spherical Fermi surface: $A'' = \frac{\partial^2}{\partial k_f^2} \pi k_f^2 = 2\pi$.

We simulate Equation 2.5 for a sample of Indium Antimonide. The simulation is displayed in Figure 2.4, and the input data used for this simulation is shown in Table 1.

g	$m_c^* = m_e^*$	μ	n	ρ	\mathcal{M}_{sample}
-50.6[9]	$0.01359m_0[9]$	$0.28 \frac{\text{n}^2}{\text{V s}}$	$5.2288 \times 10^{23} \text{ m}^{-3}$	$5.7747 \times 10^3 \frac{\text{kg}}{\text{m}^3}[9]$	0.0064 g

Table 1: Input data used for the simulation in Figure 2.4.

The value for the electron density (n), used in this simulation, has been determined from a measurement of the Hall effect, see Figure 2.3. The Hall effect occurs when both a voltage and a perpendicular magnetic field are applied to a material. The Lorentz force will cause the electrons travelling through the material to be deflected towards the edge of the material. This causes a net positive and negative charge to accumulate on the opposite edges. Therefore, there will be a voltage across the opposite edges, perpendicular to both the magnetic field and applied voltage. This voltage is called the Hall voltage and it is determined by: [6]

$$V_H = V_y = \frac{I_x B_z}{net_{sample}} \quad (2.7)$$

Here I_x is the applied current, B_z is the applied magnetic field, e is the electron charge, t_{sample} is the thickness of the sample, and n is the carrier density. Equation 2.7 shows us that we can determine the carrier density directly from the slope of Figure 2.3, we find that $n = (5.2288 \pm 0.0010) \times 10^{23} \text{ m}^{-3}$.

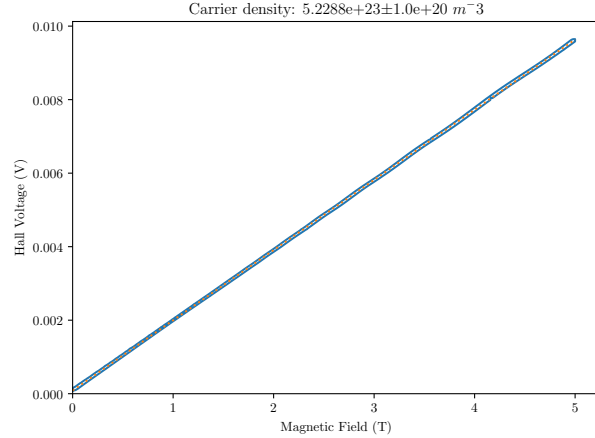


Figure 2.3: Measurement of the Hall effect of a $625 \times 10^{-6} \mu\text{m}$ thick sample of InSb using a current of 0.1 A.

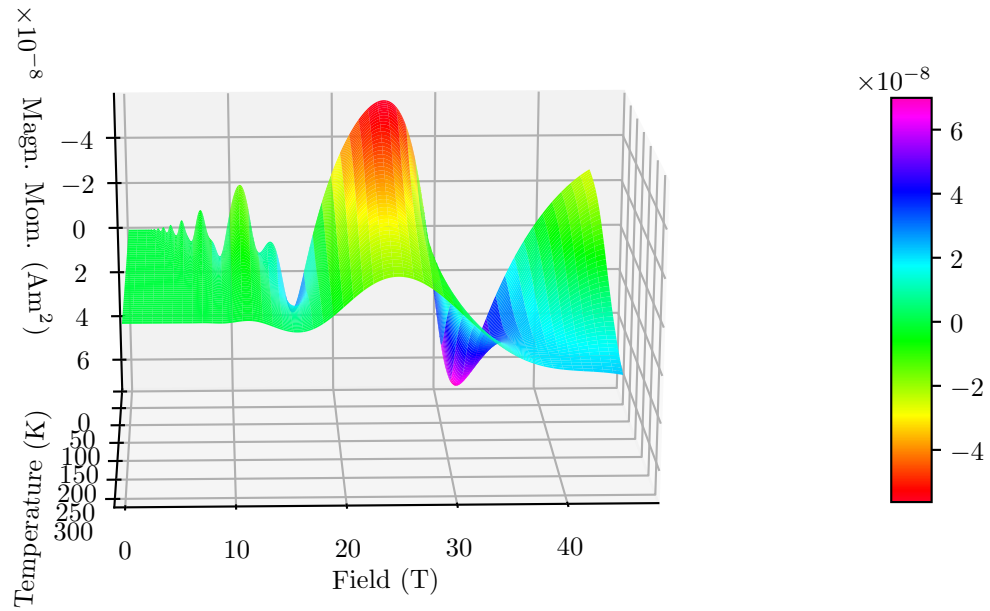


Figure 2.4: Simulation of the first 50 terms of the de-Haas-van-Alphen oscillation in Indium Antimonide as a function of magnetic moment and temperature.

As expected, Figure 2.4 shows oscillations in the magnetic moment periodic with $1/B$, the amplitude of these oscillations gets larger for larger magnetic fields B and lower temperatures T . Note that most of the parameters in Table 1 themselves depend on the temperature, thus the values shown in this table are only valid for low temperatures. Therefore, as the temperature increases, the accuracy of the simulation significantly decreases.

When we compare our simulation of the de-Haas-van-Alphen oscillations in Figure 2.4 with our measurement of the Shubnikov-de-Haas oscillations in Figure 2.2. We find that peaks occur at about the

same value for the magnetic field, we see peaks at approximately 14 T, 11 T, 7 T and 5 T. We also see that in both figures clear spin-splitting first occurs in the 7 T peak.

Having described the theoretical background, measured the Shubnikov-de-Haas oscillations, and simulated the de-Haas-van-Alphen oscillations, we now have a good idea on what to expect from a measurement of the de-Haas-van-Alphen oscillations. We will continue in the next section with describing and characterizing our setup, and attempting to perform such a measurement.

3 Torque Magnetometry

Torque magnetometry is a technique for determining the magnetization of a material by measuring the torque that a magnetized sample exerts on a cantilever in a magnetic field. A schematic is shown in Figure 3.1.

A magnetized sample on a cantilever, will exert a force on this cantilever in an attempt to position itself in the most energetically favourable position. Paramagnetic materials are attracted by magnetic fields, this effect can be observed at home by observing how metals 'stick' to magnets. Diamagnetic materials on the other hand try to expel magnetic fields from their interior and thus will be repelled by magnetic fields. Using that the energy of magnetized sample in a magnetic field is given by $U = -\vec{m} \cdot \vec{B}$ [1, 4] we can write this force as:

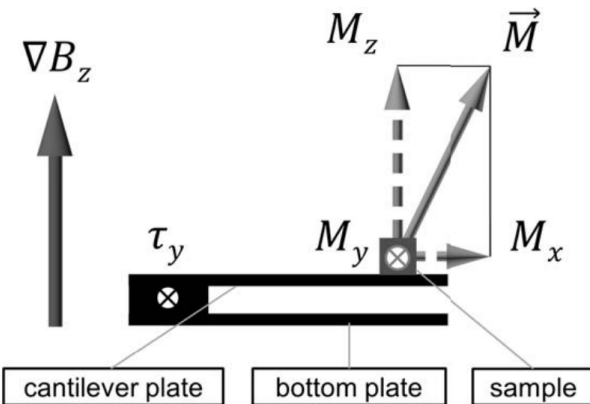


Figure 3.1: Schematic of forces on a cantilever with a sample in a magnetic field.[4]

$$\vec{F} = \vec{\nabla} (\vec{m} \cdot \vec{B}) \quad (3.1)$$

Using Figure 3.1 we see that this is the same as:

$$\vec{F} = \vec{\nabla} (m_z B_z) = \vec{\nabla} (m_{\parallel} B) \quad (3.2)$$

Equation 3.2 shows us the effect of the parallel component of the magnetic moment. However, not all materials will have their magnetic moment vectors in exactly the same direction as the applied magnetic field. This is usually caused by the material having an interesting anisotropic crystal structure. This perpendicular component exerts a torque on the cantilever, which is given by: [1, 4]

$$\vec{\tau} = \vec{m} \times \vec{B} \quad (3.3)$$

Which according to Figure 3.1 reduces to:

$$\tau_y = -m_x B_z = -m_{\perp} B \quad (3.4)$$

We would like to write both the perpendicular and parallel components in one equation, therefore we write the force in Equation 3.2 as a torque:

$$\vec{\tau} = \vec{x} \times \vec{F} = \vec{x} \times \vec{\nabla} (m_{\parallel} B) \quad (3.5)$$

Here we have defined \vec{x} as the arm of the cantilever, whose length we will define as $||\vec{x}|| \equiv L_c$. We can write Equation 3.5 a little easier by looking at Figure 3.1 and realizing that both m_{\parallel} and B can only depend on the z coordinate:

$$\tau_y = -L_c \frac{\partial (m_{\parallel} B)}{\partial z} \quad (3.6)$$

Taking Equation 3.4 and Equation 3.6 together we obtain the total torque exerted on the cantilever:

$$\boxed{\tau = -m_{\perp}B - L_c \frac{\partial(m_{\parallel}B)}{\partial z} = - \left(m_{\perp} + L_c m_{\parallel} \frac{\partial}{\partial z} \right) B} \quad (3.7)$$

Where in the second step we have assumed that m_{\parallel} does not depend on the position (z) of the sample.

We now know how the exerted torque depends on the magnetic moment. The question arise how we are actually going to measure this torque. There are in fact several ways to do this, Figure 3.1 already gives a hint to one of them.

3.1 Capacitive Measurement of Torque

In Figure 3.1 we can see the cantilever with the sample attached to it, if we look further we see that below that there is a second plate. These two plates act as a capacitor, with area A and distance d between them. The capacitance of such a capacitor is given by:

$$C_0 = \frac{\epsilon_0 A}{d} \quad (3.8)$$

However once we start applying a torque to the cantilever Equation 3.8 is no longer completely true. The cantilever bends and this causes the distance between the cantilever and the ground plate to be nonuniform along the length of the cantilever. To calculate exactly what this distance will be after applying a torque, we must first determine how the cantilever bends. To do this, we start with the Euler-Bernoulli equation, which describes the deflection of a beam upon applying a load to it:

$$\frac{d^2}{dx^2} \left(EI \frac{d^2 b}{dx^2} \right) = q = -F\delta(x - L_a) \quad (3.9)$$

Here, E is the elasticity of the cantilever, I is the second moment of area (we will calculate this later), $b(x)$ is the bending of the cantilever, and q is the distributed load (force per unit length). We assume that all the bending takes place in the arms of the cantilever, a reasonable approximation because the arms are much thinner than the rest of the cantilever. Using this approximation we can write $q = -F\delta(x - L_a)$ since the force that is bending the arms of the cantilever is only applied to the end of these arms. Here we have introduced L_a which is the length of the cantilever's arms. Integrating Equation 3.9 twice gives:

$$\begin{aligned} \frac{d}{dx} \left(EI \frac{d^2 b}{dx^2} \right) &= -F \\ \Rightarrow EI \frac{d^2 b}{dx^2} &= -Fx + c_1 \end{aligned}$$

Bringing EI to the other side and integrating twice again gives:

$$\begin{aligned} \Rightarrow \frac{d^2 b}{dx^2} &= \frac{-Fx + c_1}{EI} \\ \Rightarrow \frac{db}{dx} &= \frac{-Fx^2/2 + c_1 x}{EI} + c_2 \\ \Rightarrow b(x) &= \frac{-Fx^3/6 + c_1 x^2/2}{EI} + c_2 x + c_3 \end{aligned}$$

To find c_1, c_2, c_3 we use the boundary conditions. In $x = 0$ the bending b must also be 0 as that is where the cantilever is attached to the rest of the system, for this same reason the derivative of b must

also be 0 in this point. At the other end of the beam $x = L_a$ the second derivative of b should be 0 since the rate of change of bending no longer changes beyond this point.

$$\begin{aligned} b(0) &= 0 \implies c_3 = 0 \\ \left(\frac{db}{dx}\right)_{x=0} &= 0 \implies c_2 = 0 \\ \left(\frac{d^2b}{dx^2}\right)_{x=L_a} &= 0 \implies c_1 = FL_a \end{aligned}$$

We find that:

$$b(x) = \frac{-Fx^3/6 + FL_a x^2/2}{EI} = \frac{Fx^2}{6EI} (3L_a - x) \quad (3.10)$$

We are interested in the vertical position of the capacitive part of the cantilever, which starts at the end of the arms. Because we assume the capacitive part of the cantilever does not bend, we can describe its position with a linear equation. Therefore, we would like to know both the displacement and the slope of the arm at its end:

$$b(L_a) = b_{max} = \frac{FL_a^3}{3EI} \quad (3.11)$$

$$\left(\frac{db}{dx}\right)_{x=L_a} = a = \frac{FL_a^2}{2EI} \quad (3.12)$$

From this it follows that the distance between the capacitive plates can be described as follows:

$$d(x) = d_0 - \frac{FL_a^2}{2EI} x + b_{offset}$$

Where d_0 is the distance between the plates when no force is applied. We can determine b_{offset} by using that we know that $d(L_a) = d_0 - b_{max} = d_0 - \frac{FL_a^3}{3EI}$

$$\begin{aligned} d(L_a) &= d_0 - \frac{FL_a^3}{3EI} = d_0 - \frac{FL_a^3}{2EI} + b_{offset} \implies b_{offset} = -\frac{FL_a^3}{3EI} + \frac{FL_a^3}{2EI} = \frac{FL_a^3}{6EI} \\ d(x) &= d_0 - \frac{FL_a^2}{2EI} x + \frac{FL_a^3}{6EI} \end{aligned} \quad (3.13)$$

Now that we know the distance between the plates as a function of x we can calculate the capacitance by writing Equation 3.8 as an integral:

$$C_1 = \int_{L_c-r}^{L_c+r} \frac{\epsilon_0 w(x)}{d(x)} dx \quad (3.14)$$

Here L_c is the centre of the cantilever's capacitive plate. This coincides with L_c in Equation 3.6 because the point where the torque is applied should be the centre of the plate. The capacitive plate of the cantilever is a circle, thus the width $w(x)$ is equal to $2\sqrt{r^2 - (x - L_c)^2}$. Plugging this into Equation 3.14 gives:

$$C_1 = \int_{L_c-r}^{L_c+r} \frac{\epsilon_0 2\sqrt{r^2 - (x - L_c)^2}}{d_0 - \frac{FL_a^2}{2EI} x + \frac{FL_a^3}{6EI}} dx \quad (3.15)$$

A step-by-step solution of Equation 3.15 can be found in Appendix A, the final result is:

$$C_1 = \frac{\epsilon_0 A}{d_0 - \frac{FL_a^3}{3EI}} \quad (3.16)$$

Note that Equation 3.16 reduces to Equation 3.8 if $F = 0$ as it should. Next we determine the second moment of area I . Because our cross-section is in the y - z plane this is given by:

$$I = \int \int z^2 dy dz = 2 \int_{-t/2}^{t/2} \int_{\lambda/2-v/2}^{\lambda/2+v/2} z^2 dy dz \quad (3.17)$$

We multiply by 2 because we have two arms. λ represents the separation between the centroid axis of both arms, v is the width of the arms, and t is the thickness of the arms. See Appendix C for a schematic of the cantilevers. Therefore the separation between the edges of the arms is equal to $\lambda - v$. The solution to this integral is:

$$I = 2 [y]_{\lambda/2-v/2}^{\lambda/2+v/2} \left[\frac{z^3}{3} \right]_{-t/2}^{t/2} = \frac{2}{3} \left(\frac{\lambda}{2} + \frac{v}{2} - \left(\frac{\lambda}{2} - \frac{v}{2} \right) \right) \left(\frac{t^3}{8} - \frac{(-t)^3}{8} \right) \quad (3.18)$$

$$\implies I = \frac{vt^3}{6} \quad (3.19)$$

Plugging Equation 3.19 into Equation 3.16 gives:

$$C_1 = \frac{\epsilon_0 A}{d_0 - \frac{FL_a^3}{3E \frac{vt^3}{6}}} \quad \boxed{C_1 = \frac{\epsilon_0 A}{d_0 - \frac{2FL_a^3}{Ev t^3}}} \quad (3.20)$$

We know that any bending of the cantilever is small compared to d_0 . Therefore we can once again apply a Taylor expansions:

$$C_1 = \frac{\epsilon_0 A}{d_0 - \Delta d} \approx \frac{\epsilon_0 A}{d_0} + \frac{\epsilon_0 A}{d_0^2} \Delta d + \mathcal{O}((\Delta d)^2)$$

$$C_1 = \frac{\epsilon_0 A}{d_0} + \frac{\epsilon_0 A}{d_0^2} \frac{2FL_a^3}{Ev t^3} \quad (3.21)$$

From this it follows that any force applied to the cantilever leads to a change in capacitance as follows:

$$\Delta C = C_1 - C_0 = \frac{\epsilon_0 A}{d_0^2} \frac{2FL_a^3}{Ev t^3} F \quad (3.22)$$

$$\implies F = \frac{d_0^2}{\epsilon_0 A} \frac{Ev t^3}{2L_a^3} \Delta C$$

Writing this in terms of torque gives:

$$\vec{\tau} = \vec{x} \times \vec{F} = \vec{x} \times \hat{z} \frac{d_0^2 Ev t^3}{2\epsilon_0 A L_a^3} \Delta C \quad (3.23)$$

Here we have introduced \hat{z} because we know that the force on the cantilever must be in the z -direction. We can further simplify Equation 3.23 to:

$$\tau = \tau_y = -L_c \frac{d_0^2 Ev t^3}{2\epsilon_0 A L_a^3} \Delta C \quad (3.24)$$

Combining Equation 3.7 and Equation 3.24, and using that $L_c = L_a + r$ gives:

$$(L_a + r) \frac{d_0^2 Ev t^3}{2\epsilon_0 A L_a^3} \Delta C = m_\perp B + (L_a + r) \frac{\partial(m_\parallel B)}{\partial z} \quad (3.25)$$

$$\Rightarrow \Delta C = \frac{2\epsilon_0 A L_a^3}{Evd_0^2 t^3} \left(\frac{m_\perp}{L_a + r} + m_\parallel \frac{\partial}{\partial z} \right) B \quad (3.26)$$

Equation 3.26 shows us that we can calculate the perpendicular component of the magnetic moment if we measure the change in capacitance between before and after magnetizing the sample, in a region where $\partial B / \partial z = 0$. Once we have obtained the perpendicular component we can repeat the measurement in a region where $\partial B / \partial z \neq 0$ and use the now known m_\perp to calculate the parallel component of the magnetic moment. Note that the magnetization M is obtained by dividing the magnetic moment m by the volume V of the sample.

3.2 Other Ways to Measure Torque

We have described here in detail how to measure the exerted torque using capacitance, this is in fact the most common method. However, as stated before, it is in principle possible to measure the torque using different methods. For instance, one could measure the torque using a **piezoelectric cantilever**. A voltage will appear across such a cantilever directly corresponding with bending of the cantilever and therefore with the torque. Another possible method uses **optical interferometry**. In this method one shoots a laser on the cantilever, and records the interference pattern between this laser beam and the reflected beam. When a torque is exerted on the cantilever, any displacement of this cantilever larger than half the laser wavelength will cause a observable shift in the interference pattern.

3.3 Setup at HFML



Figure 3.2: The probe, the tip is shown separately in Figure 3.3b, also shown is an Andeen-Hagerling 2700A capacitance bridge on the left.

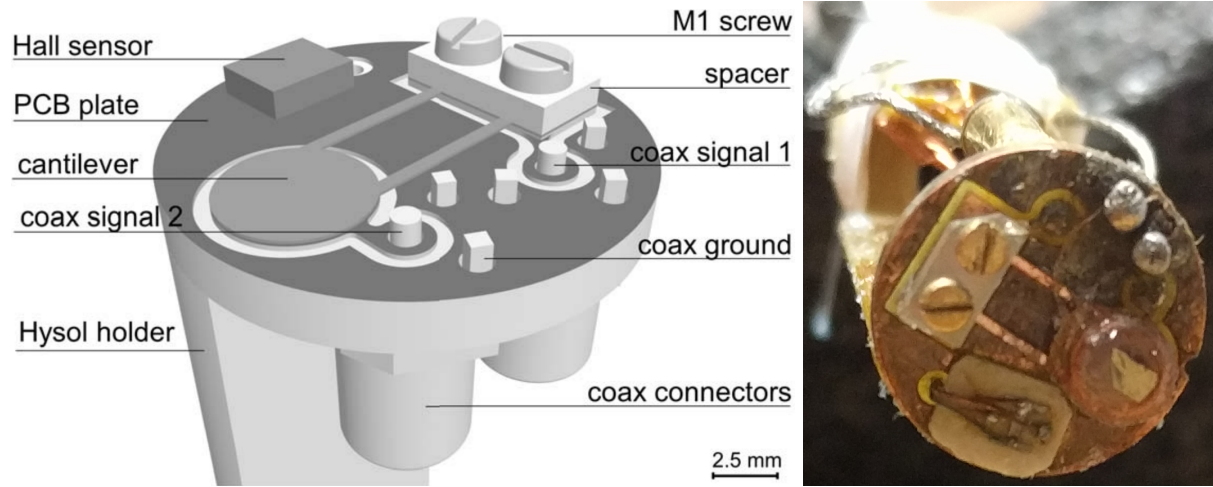
The basic (DC) torque magnetometry setup consists of a cantilever attached with two screws to the end of the probe. A spacer ensures that there is some separation between the cantilever and the base plate, see Figure 3.3a. The capacitance can then be measured with an Andeen-Hagerling 2700A capacitance bridge (Figure 3.2) from two BNC coax connectors at the top of the probe.

Furthermore, a Hall sensor is also attached to the tip of the probe (see Figure 3.3) in order to determine the actual magnetic field when the tip of the probe is not in the magnets field centre. The Hall sensor has 4 terminals, a sinusoidal voltage is applied to two opposite terminals by grounding one terminal and connecting the other to the sinus output of a SR830 lock-in amplifier. When a magnetic field is applied to the Hall sensor, the Hall effect will cause a voltage across the other two perpendicular terminals, which can be measured on the lock-in amplifier. The voltage across the Hall sensor is linear with the applied magnetic field, and is also described by Equation 2.7 which we saw before when we determined the carrier density of our sample.

A thermometer is also attached to the probe slightly above the tip. The temperature is then measured using a LakeShore 335 cryogenic temperature controller.

To measure with oscillating cantilever magnetometry (AC) instead, a coil is glued onto the cantilever, see Figure 3.3b. The coil, as well as the Hall sensor and thermometer, is wired to a Fischer 16 connector at the top of the probe, where the coil can be driven by any AC current source.

The whole probe is inserted into an anti-cryostat which in turn is inside a superconducting magnet. For our experiments we use one of HFML's superconducting magnets (SC2). This magnet can go up to 15 T and has a homogeneity of $<1 \times 10^{-4}$ in 1 cm DSV ([3] for more specifications).



(a) Schematic of our torque magnetometry setup, for cantilever magnetometry we glue a coil on top of the cantilever. [4] (b) The bottom of the probe, visible are a coil with a InSb sample on top, and the Hall sensor below it

Figure 3.3

3.4 Setup Characterization

3.4.1 Field Profile

We start with a large coil consisting of 1000 windings of 30 μm diameter copper wire, with a radius of 1.5 mm. The magnetic moment of such a coil is given by:

$$m = NIA = 1000I\pi r^2 = 0.007 \text{ m}^2 I \quad (3.27)$$

First, we determine the field profile of the magnet by applying a sinusoidal voltage of 0.04 V to two opposing terminals of the Hall sensor and measuring the resulting voltage on the other two terminals with a Lock-In Amplifier. We set our magnet's magnetic field to be constant at 5 T, send a current of 10 mA at 0.05 Hz through the coil, and move our probe through the magnet. As we do this, the resulting Hall voltage over the Hall sensor will vary linearly with the strength of the magnetic field. And thus we find the strength of the magnetic field as a function of the system's position inside the magnet, in other words: the field profile. The results are shown in Figure 3.4, we see that the value of the magnetic field can be approximated by a parabola with its maximum at the field centre. We write this approximation as follows:

$$B(z) = B_0 \left(1 - \frac{z^2}{z_0^2} \right) \quad (3.28)$$

Here B_0 is the magnetic field in the field centre ($z = 0$), we know this should be equal to 5 T. And $z = z_0$ is the point where our parabolic approximation is zero. Note that in general the actual field is

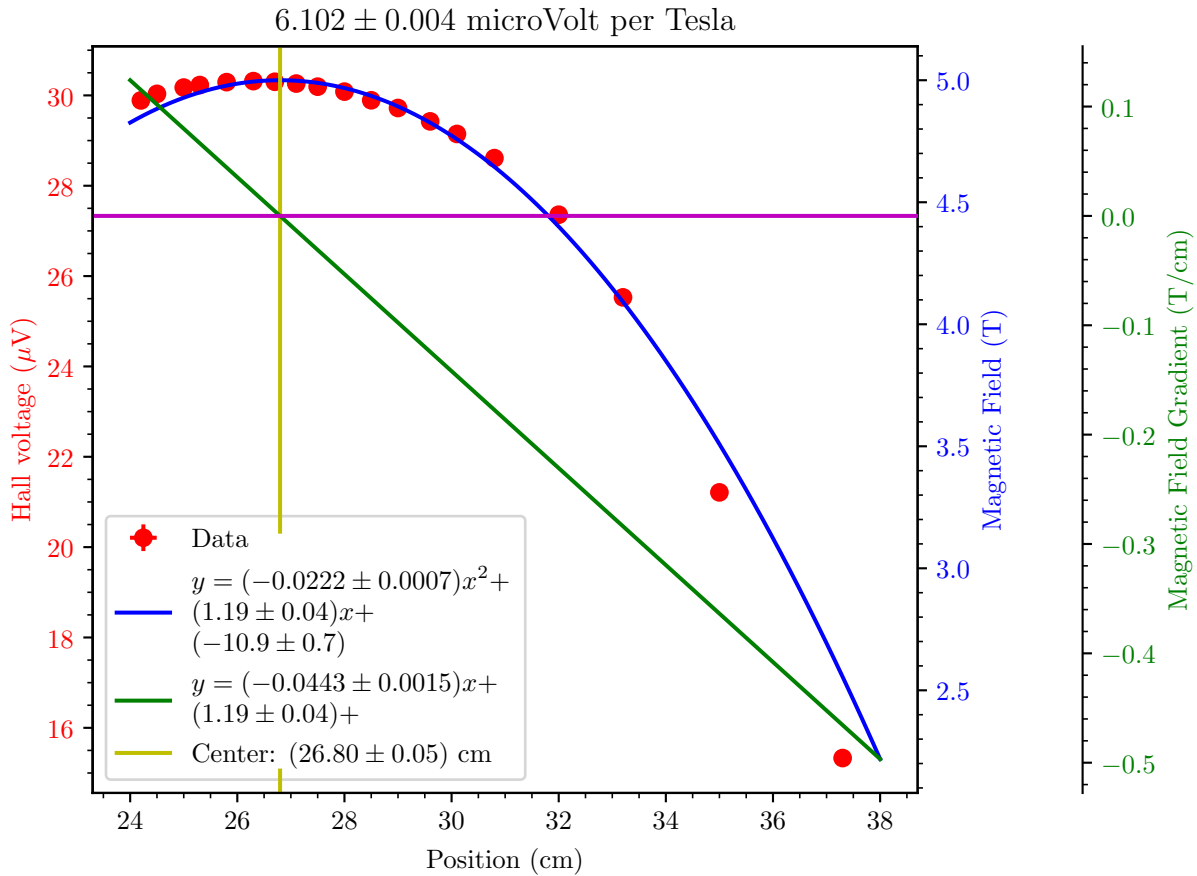


Figure 3.4: Field profile of HFML's SC2 at 5 T and 23 K

not zero in $z = z_0$ because our approximation is only valid for $z \ll z_0$.

Due to gravity pulling on the cantilever, coil and sample, the whole system will be slightly at an angle with respect to the base plate. We can determine both this angle and the sensitivity of the system, by measuring the amplitude of the oscillations in the capacitance as a function of the position of the whole system in the magnetic field. The position in the field determines both the value of the magnetic field and the gradient of the magnetic field over the system.

While measuring the field profile, we also send a sinusoidal current through the coil, the resulting oscillations in the capacitance are shown in Figure C.1. After fitting a sine through this data, we plot the amplitude, frequency and equilibrium positions of each sine as a function of the position in the magnet in Figures 3.5, 3.6a and 3.6b. Here we have shifted the x-axis such that 0 corresponds with the centre of the magnet where the magnetic field is at its maximum. We have also fitted a parabola through Figure 3.5, which will enable us to find both the angle and sensitivity of the cantilever plus coil system. In order to do this, we start with plugging the parabolic approximation for the magnetic field into Equation 3.26, which gives:

$$\Delta C = \frac{2\epsilon_0 A L_a^3}{Evd_0^2 t^3} \left(\frac{m_\perp}{L_a + r} + m_\parallel \frac{\partial}{\partial z} \right) B_0 \left(1 - \frac{z^2}{z_0^2} \right) \quad (3.29)$$

$$\implies \Delta C = \frac{2\epsilon_0 A L_a^3}{Evd_0^2 t^3} \left(\frac{m_\perp}{L_a + r} \left(1 - \frac{z^2}{z_0^2} \right) - m_\parallel \frac{2z}{z_0^2} \right) B_0 \quad (3.30)$$

From Equation 3.30 we learn that the linear part of our parabolic fit in Figure 3.5 corresponds to

m_{\parallel} and the other two terms correspond to m_{\perp} . We can use this to determine the angle of our cantilever using the fit in Figure 3.5. First we write Equation 3.30 a bit simpler:

$$\Delta C = \alpha B_0 \left(m_{\perp} \left(1 - \frac{z^2}{z_0^2} \right) - m_{\parallel} \frac{2z(L_a + r)}{z_0^2} \right) \quad (3.31)$$

Where we have introduced α to collect all prefactors.

$$\alpha \equiv \frac{2\epsilon_0 A L_a^3}{Evd_0^2 t^3 (L_a + r)} \quad (3.32)$$

Using Figure 3.5 we can write Equation 3.31 term by term as:

$$\begin{aligned} \alpha B_0 m_{\perp} &= (0.00549 \pm 0.00004) \text{ pF} \\ -\alpha B_0 m_{\parallel} \frac{2z(L_a + r)}{z_0^2} &= (-0.00013 \pm 0.00002) \text{ pF cm}^{-1} z \\ -\alpha B_0 m_{\perp} \frac{z^2}{z_0^2} &= (-0.000033 \pm 0.000002) \text{ pF cm}^{-2} z^2 \end{aligned}$$

We use that $z_0 = 15.08 \text{ cm}$ (which is the root of our fit polynomial in Figure 3.4) and $L_a + r = 0.625 \text{ cm}$ and find that:

$$\alpha B_0 m_{\perp} = (0.00549 \pm 0.00004) \text{ pF}$$

$$\alpha B_0 m_{\parallel} = (0.023 \pm 0.004) \text{ pF}$$

$$\alpha B_0 m_{\perp} = (0.0075 \pm 0.0005) \text{ pF}$$

Taking the weighted average of the first and third equation we get:

$$\alpha B_0 m_{\perp} = (0.00550 \pm 0.00004) \text{ pF}$$

$$\alpha B_0 m_{\parallel} = (0.023 \pm 0.004) \text{ pF}$$

Writing this in terms of $||\vec{m}|| = m$ and the angle ϕ gives:

$$\alpha B_0 m \sin(\phi) = (0.00550 \pm 0.00004) \text{ pF}$$

$$\alpha B_0 m \cos(\phi) = (0.023 \pm 0.004) \text{ pF}$$

Dividing the first equation by the second gives:

$$\tan(\phi) = 0.24 \pm 0.05$$

From this it follows that:

$$\phi = 0.23 \pm 0.04 = (13 \pm 2)^\circ \quad (3.33)$$

Furthermore, we can also find an expression for $m = \sqrt{m_{\parallel}^2 + m_{\perp}^2}$:

$$m = \frac{(0.0047 \pm 0.0008) \text{ pF T}^{-1}}{\alpha}$$

Where we have used that $B_0 = 5 \text{ T}$.

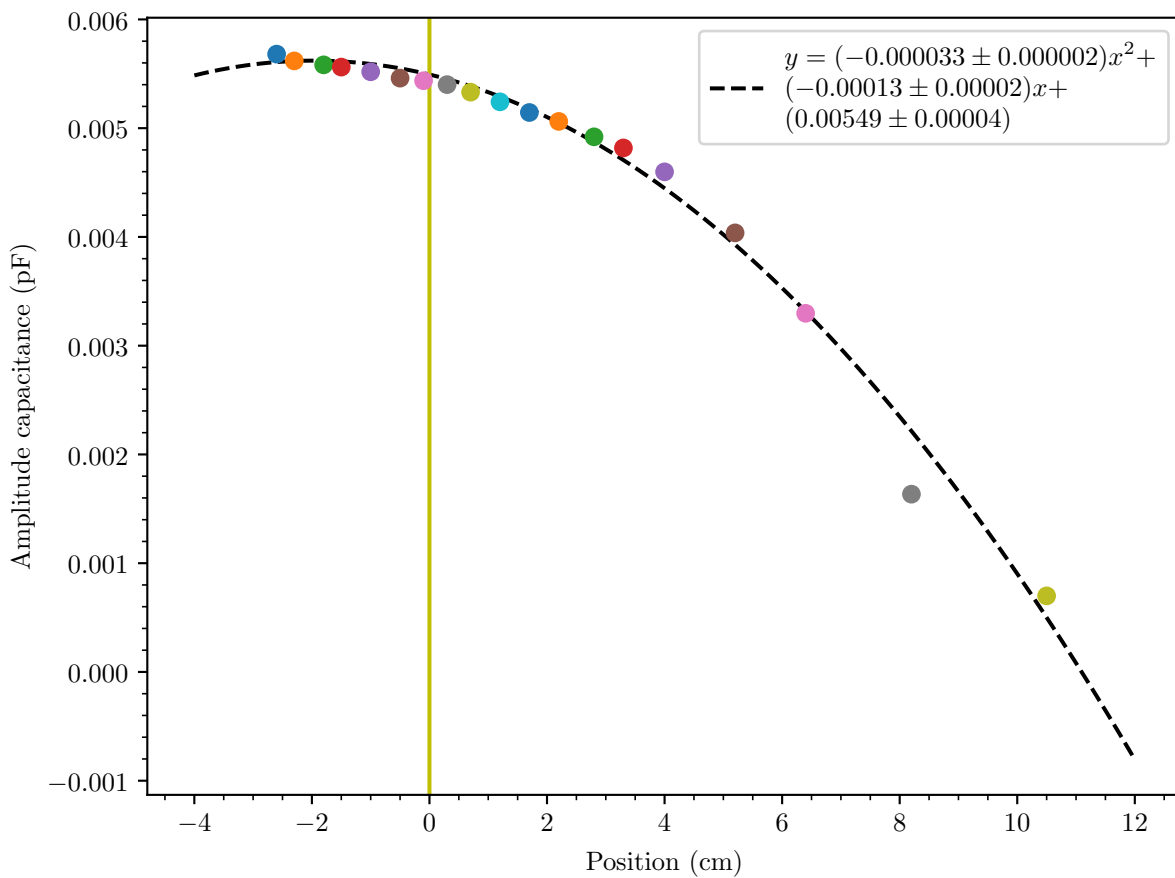
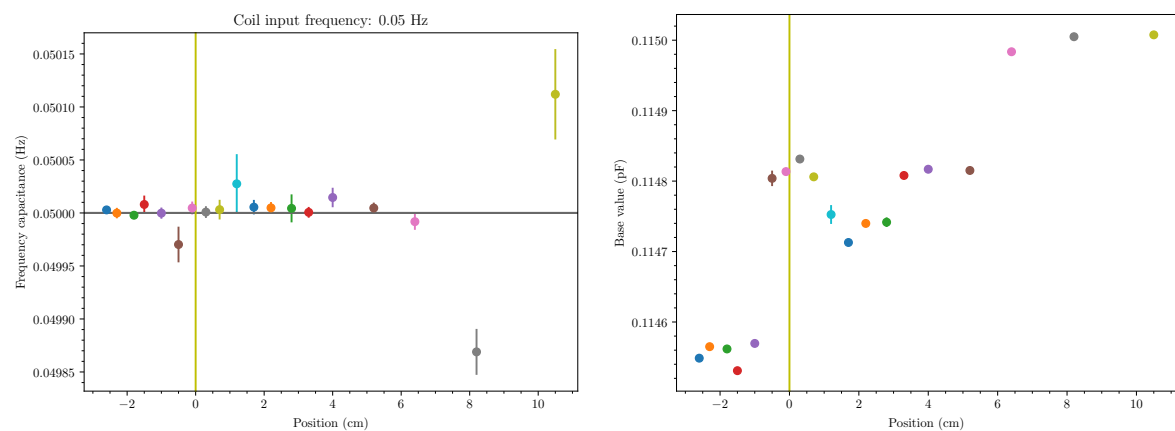


Figure 3.5: Amplitude of the fitted sine from Figure C.1 at 5 T and 4.2 K, the position axis has been adjusted to be relative to the field centre.



(a) Frequency of the fitted sine from Figure C.1 at 5 T and 4.2 K, the position axis has been adjusted to be relative to the field centre.
(b) Equilibrium position of the fitted sine from Figure C.1 at 5 T and 4.2 K, the position axis has been adjusted to be relative to the field centre.

Figure 3.6

We also know what the magnetic moment should be from Equation 3.27. Plugging Equation 3.27 in, and using that $I = 10 \text{ mA}$ we get:

$$7.07 \times 10^{-5} \text{ A m}^2 = \frac{(0.0047 \pm 0.0008) \text{ pF T}^{-1}}{\alpha}$$

From this it follows that:

$$\alpha = (67 \pm 11) \frac{\text{pF}}{\text{A m}^2 \text{T}} = (67 \pm 11) \frac{\text{pF}}{\text{N m}} \quad (3.34)$$

As a sanity check, we can use Equation 3.32 and the information in Appendix C to obtain an educated guess for what α should approximately be. We correct the elastic modules from Appendix C using Equation 3.35[2], here E_0 is the elastic modules at 0K and T_{\max} is the melting temperature for the material:

$$\frac{E(T)}{E_0} = 1 - 0.2 \frac{T}{T_{\max}} - 0.25 \left(\frac{T}{T_{\max}} \right)^2 \quad (3.35)$$

We also correct d_0 by using the angle we just calculated: $d_0 + L_a \tan(\phi)$. We find that $E(4.2 \text{ K}) = 146 \text{ GPa}$ and that $d_0 = 1.0 \text{ mm}$. Plugging all this into Equation 3.32 gives $\alpha = 83 \frac{\text{pF}}{\text{A m}^2 \text{T}}$, which is actually quite close to what we find from the data.

Furthermore, from Figure 3.6a and C.1 we see that, as we increase the distance from the field centre, we increase the errors in the fitting. This is likely due to the increased field gradient at larger distances from the field centre. A larger field gradient increases the non-linearity of the cantilever, as the difference between the magnetic fields it experiences in the two extrema of the oscillation increases.

Also, Figure 3.6b shows us that the equilibrium position of the oscillation is not constant. However, there does not appear to be a clear trend, other than that further from the field centre the capacitance increases. This means that the distance between the cantilever and the base plate decreases, further from the field centre (smaller field, larger field gradient).

3.4.2 Linearity of the Cantilever

Next we measure the dependency of the cantilever's oscillation on the amplitude of the current we send into the coil. As we change the current through the coil, we change the magnetic moment of the coil, and therefore this will also provide us with a numerical value for the sensitivity. We set the position of the probe 7 mm below the field centre, and set the magnetic field to 15 T. Next we start changing the current through the coil, the resulting changes in the oscillation of the cantilever are shown in Figure C.2. Once again, we fit a sine through the data, and plot the amplitude, frequency and equilibrium positions of each sine in Figures 3.7, 3.8a and 3.8b.

In Figure 3.7 we see that the amplitude of the cantilever's oscillations depends linearly on the amplitude of the current oscillations sent through the coil. At about 2.25 mA we see a deviation from this linear behaviour, which indicates that the linear regime of the cantilever ends here. After making a linear fit through the data points in Figure 3.7 we can once again calculate α using a different method than we used in the previous section. From our fit in Figure 3.7 we learn that:

$$\Delta C = (34.72 \pm 0.07) \frac{\text{pF}}{\text{A}} I$$

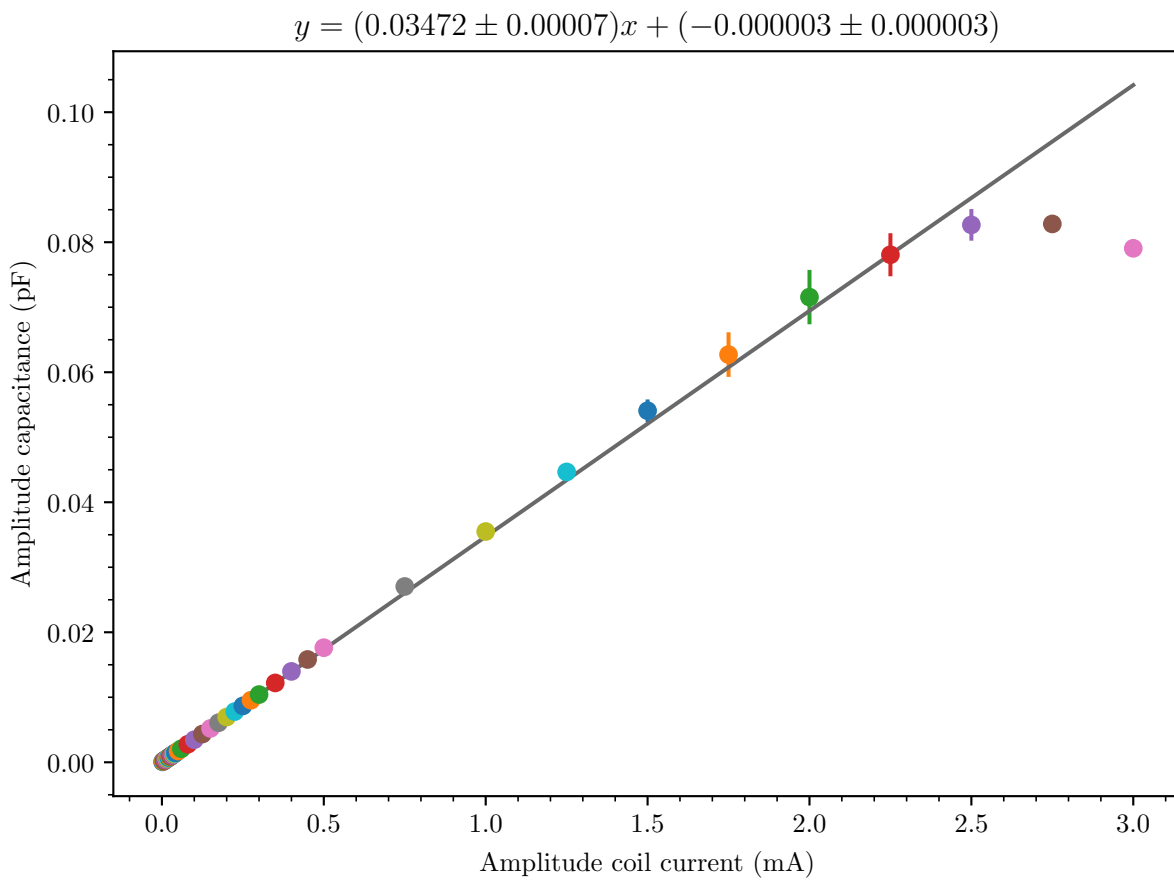
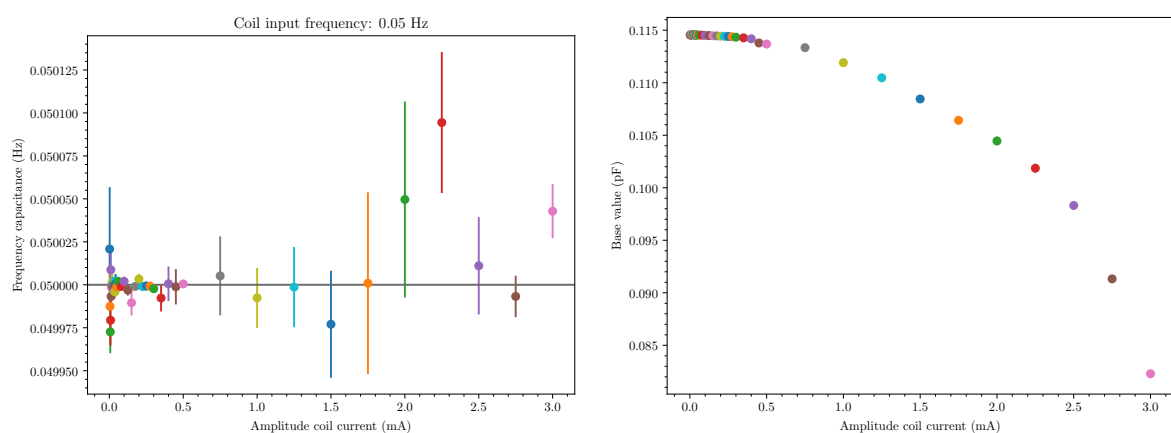


Figure 3.7: Amplitude of the fitted sine from Figure C.2 at 15 T and 4.2 K.



(a) Frequency of the fitted sine from Figure C.2 at 15 T and 4.2 K.
(b) Equilibrium position of the fitted sine from Figure C.2 at 15 T and 4.2 K.

Figure 3.8

Using Equation 3.27 we find that:

$$\Delta C = (4912 \pm 10) \frac{\text{pF}}{\text{A m}^2} m$$

Combining this with Equation 3.31 and writing $m_{\perp} = m \sin(\phi)$ and $m_{\parallel} = m \cos(\phi)$ gives:

$$\alpha B_0 \left(m \sin(\phi) \left(1 - \frac{z^2}{z_0^2} \right) - m \cos(\phi) \frac{2z(L_a + r)}{z_0^2} \right) = (4912 \pm 10) \frac{\text{pF}}{\text{A m}^2} m$$

Once again we use that $L_a + r = 0.625 \text{ cm}$, $z_0 = 15.08 \text{ cm}$, $z = 0.7 \text{ cm}$ and $B_0 = 15 \text{ T}$. We also us the angle obtained in the previous section (Equation 3.33):

$$\alpha(3.4 \pm 0.6) \text{ T} = (4912 \pm 10) \frac{\text{pF}}{\text{A m}^2}$$

$$\Rightarrow \alpha = (1.5 \pm 0.3) \times 10^3 \frac{\text{pF}}{\text{Nm}} \quad (3.36)$$

This is not the same as Equation 3.34 because, as we see from Figure 3.7 we have pushed the cantilever beyond the linear regime. Beyond this linear regime forces on the cantilever tend to permanently deform it. Analysis of the cantilever under a microscope confirmed that this severely damaged the cantilever. The arms of the cantilever were badly deformed and the cantilever itself was no longer aligned with the base capacitive plate. This damage causes the cantilever's elasticity and second moment of area to be very different from what it initially was, which explains the difference in coefficient found in Equations 3.34 and 3.36.

Furthermore, Figure 3.8a shows us that as we increase the amplitude of the current, we increase the errors in the fitting. This is likely due to that larger currents cause larger oscillations, which decreases the linearity of the cantilever.

Figure 3.8b tells us that more current decreases the equilibrium position of the cantilever's oscillation. This means that as the current is increased, the distance between the plates is also increased.

3.4.3 Smaller coils

Since we broke the previous cantilever, we repeat the experiment in the above two sections for a smaller coil of 50 windings on a new cantilever. The number of windings has been chosen such that the coil has about the same magnetic moment as the sample of 0.0064 g of InSb which is also glued onto the cantilever. Equation 3.27 shows us that when we send a current of 1 mA through this coil, we get a magnetic moment of $1.1 \times 10^{-7} \text{ A m}^2$. And from the simulation in Figure 2.4 we learn that the sample has a magnetic moment of approximately $4 \times 10^{-8} \text{ A m}^2$ at 15 T. The results of both, the measurement as a function of the position inside the magnet, and of the measurement as a function of the current through the smaller coil, are shown in the figures below.

Figure 3.9 shows the amplitude of the cantilevers oscillations as a function of the cantilevers height, similar to Figure 3.5 for the larger coil. Sadly, the data (Figure C.3) is too noisy to decently fit a parabola through the data points. Therefore, we cannot obtain a calibration parameter α from this plot. This leaves us unable to find the angle between the cantilever and base plate as we did in the previous section for the coil of 1000 windings. Therefore, we will assume that the angle is zero in the consecutive calculations. Considering that the smaller coil consists of 20 times less windings, and is therefore significantly lighter, the angle is likely to be small anyway. The general trend of the data points in Figure 3.9 does appear to be correct when comparing it to Figure 3.5, in both figures the

(negative) data points above the field centre are higher then the (positive) data points below the field centre.

Figure 3.11 shows us the relation between the amplitude of the sinusoidal current sent through the coil, and the amplitude of the resulting oscillations of the cantilever. Similarly to what we did for Figure 3.7 in the previous section, we can use the slope of $(0.000\,048\,6 \pm 0.000\,001\,3) \frac{\text{pF}}{\text{mA}}$ of the linear fit in Figure 3.11 to find the calibration parameter $\alpha = (8.10 \pm 0.22) \times 10^3 \frac{\text{pF}}{\text{N}\cdot\text{m}}$, where we have assumed that the angle ϕ of the cantilever is 0.

We therefore find that our system is about 120 times more sensitive with the 20 times smaller coil. However, when we look at Figures 3.10a and 3.12a we also see that the measurement is significantly more noisy when compared to Figures 3.6a and 3.8a. In fact, the averaging on the Capacitance Bridge had to be increased to maximum to get any meaningful data at all, which is why the frequency of the current had to be reduced from 0.05 Hz to 0.01 Hz, more on that later in Section 5.

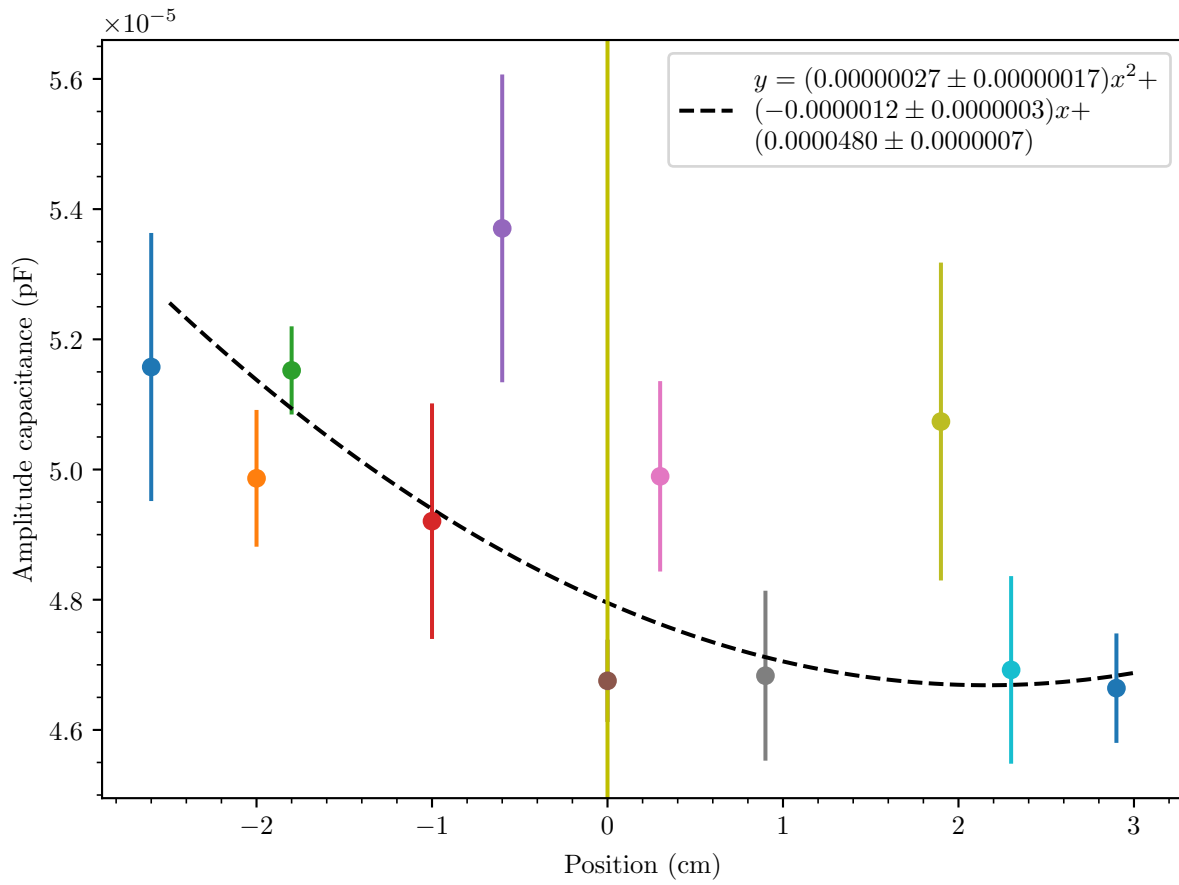
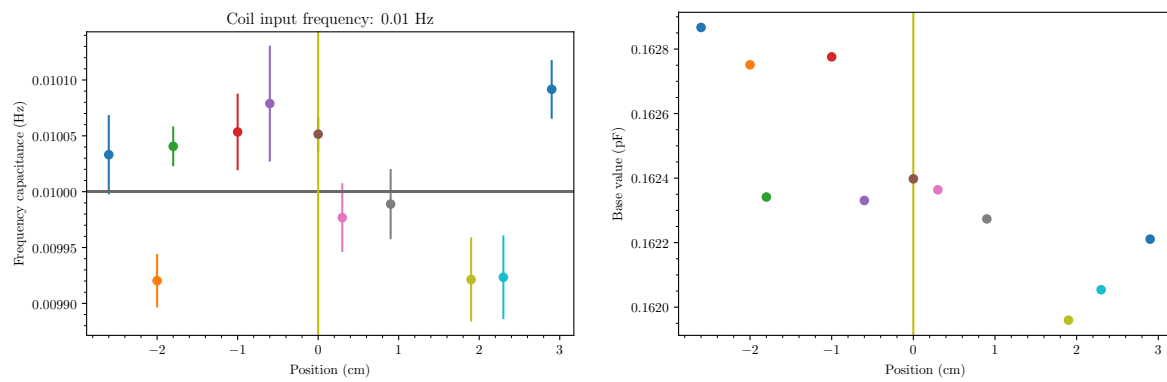


Figure 3.9: Amplitude of the fitted sine from Figure C.3 at 5 T and 4.2 K, the position axis has been adjusted to be relative to the field centre.



- (a) Frequency of the fitted sine from Figure C.3 at 5 T and 4.2 K, the position axis has been adjusted to be relative to the field centre.
(b) Equilibrium position of the fitted sine from Figure C.3 at 5 T and 4.2 K, the position axis has been adjusted to be relative to the field centre.

Figure 3.10

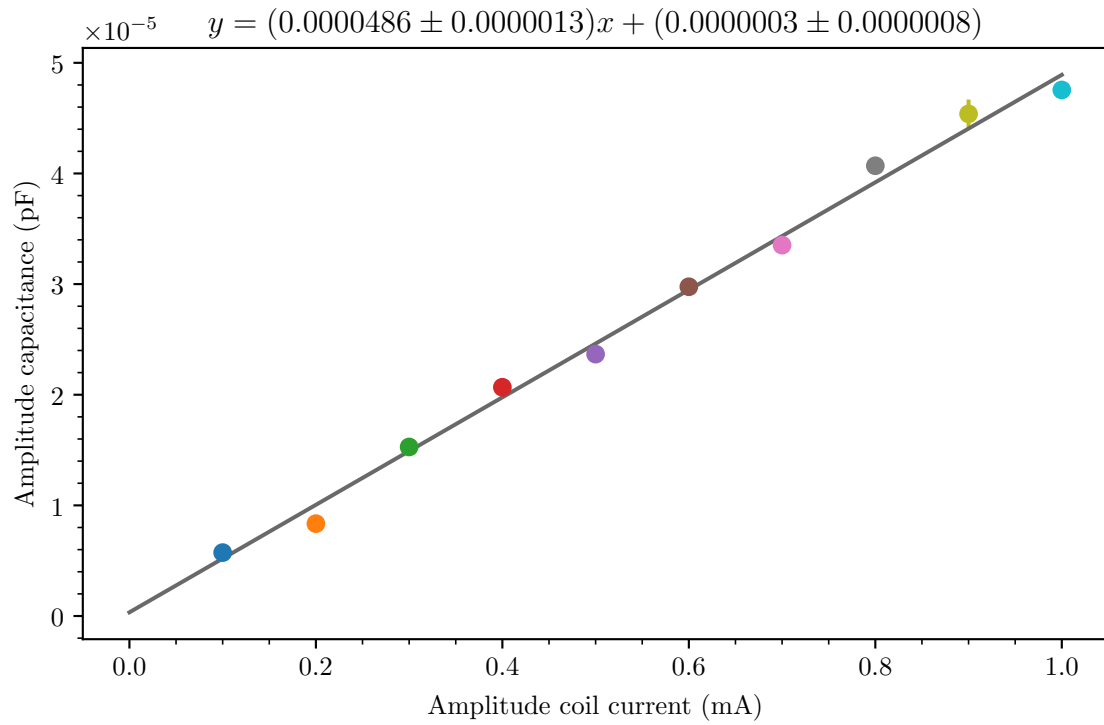


Figure 3.11: Amplitude of the fitted sine from Figure C.4 at 5 T and 4.2 K.

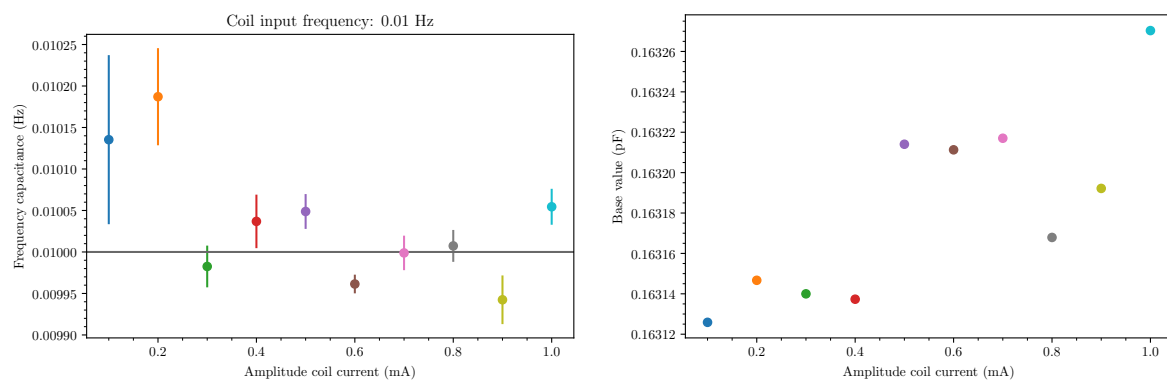


Figure 3.12

3.5 De-Haas-van-Alphen effect

To see if we can measure the magnetic moment of the sample of InSb we measure the capacitance as a function of the magnetic field. InSb exhibits quantum oscillations, which we have simulated in Figure 2.4. Equation 4.3 tells us that the amplitude is inversely dependent on the gradient of the force exhibited by the sample, therefore the sample has been positioned 1 cm below the field centre where both the field gradient and its derivative are non-zero. Analysing Equation 4.3 leads us to expect that the amplitude of the cantilever's oscillation will drop slightly when the quantum oscillations in the magnetization reach a maximum or minimum. Figures 3.13 and 3.14 show the result of the measurements, sadly we do not see clear quantum oscillations. The change in amplitude seems to be entirely dominated by the linear increase that arises from the magnetic moment from the coil. Later on we will see that this is consistent with our simulations (Figures 4.2 and 4.3). The mechanics of the problem make that the amplitude scales linearly with the sinusoidal force from the coil F_0 , while the effect of the sample is only exerted through the inverse of the *derivative* of F_1 which is significantly smaller, see Equation 4.3.

Figures 4.5 and 4.6 tell us that the quantum oscillations should be more clearly visible in the phase shift between the sinusoidal current input, and the output sinusoidal oscillations in the capacitance. However, such a phase sensitive measurement would require a lock-in amplifier, and way higher frequencies than have been used here.

Furthermore, these quantum oscillations should also be more visible in the shift in resonant frequency of the system, as shown by Figures 4.7 and 4.8. However, the use of the Andeen-Hagerling capacitance

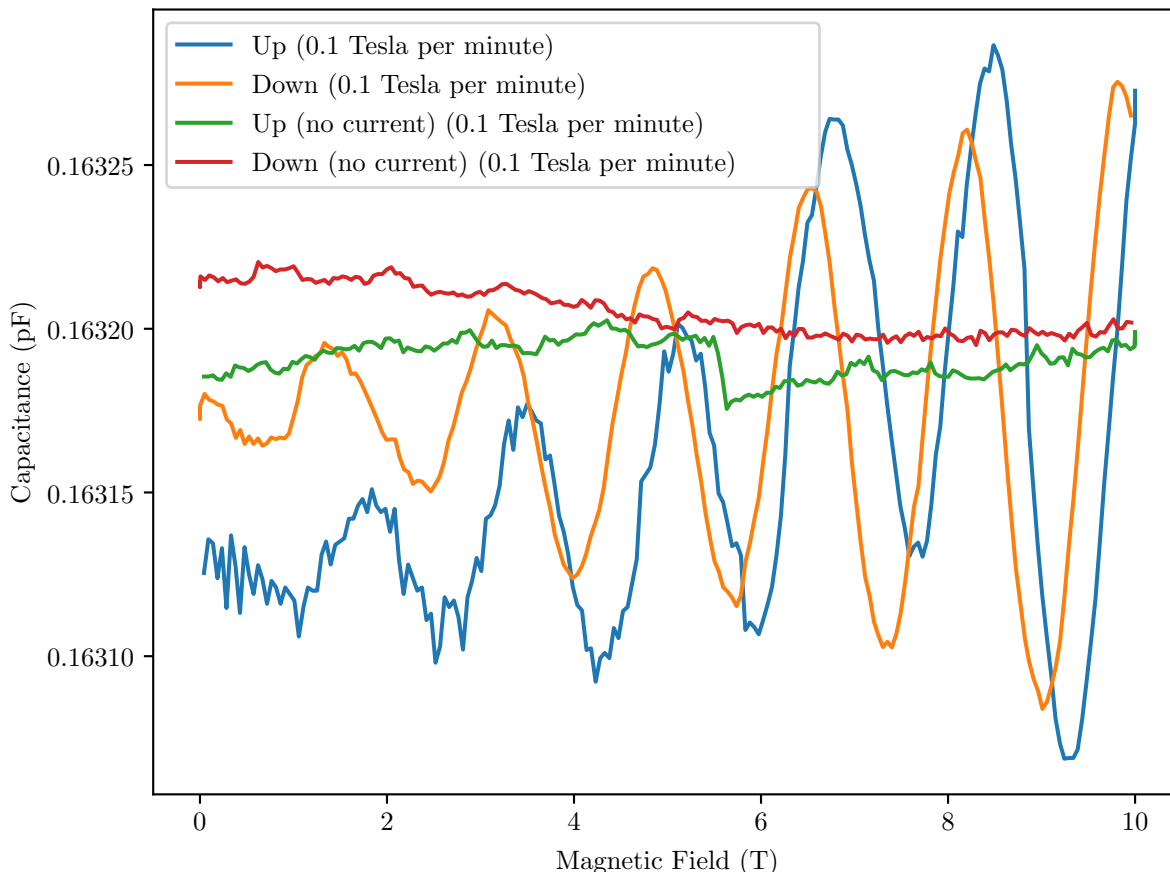


Figure 3.13: Field sweeps of 0.0064 g of InSb, while sending a sinusoidal current of 1 mA at 10 mHz through the coil, at 4.2 K.

bridge limits us to using very low frequencies, and prevents us from reaching the resonant frequency which is of the order 1.5×10^5 Hz. While the Andeen-Hagerling capacitance bridge can measure at frequencies up to 20 kHz, it also averages over many data points to achieve the accuracy needed for a noise-free measurement. This, combined with that we need to have a couple of data points within each oscillation of the current input, limits us in practice to using frequencies of the order of 10 mHz for the current input.

There are also some jumps and drifts in the signal we measured in Figures 3.13 and 3.14, these jumps could have many causes. The cantilever is very sensitive, any mechanical or electrical disturbance affects it. This makes it very difficult to avoid these jumps in data sets which are recorded over long periods of time, such as the field sweeps in Figure 3.14. Such jumps were also present in the previous measurements. However, they appear less prominent in those result due to the fact that we fitted a sine through the data points and plotted the amplitude and frequency of that fit, and due to the shorter time span of each individual measurement. For those measurements the jumps and drifts are visualized in Figures 3.6b, 3.8b, 3.10b and 3.12b where we have plotted the values the oscillations oscillate around.

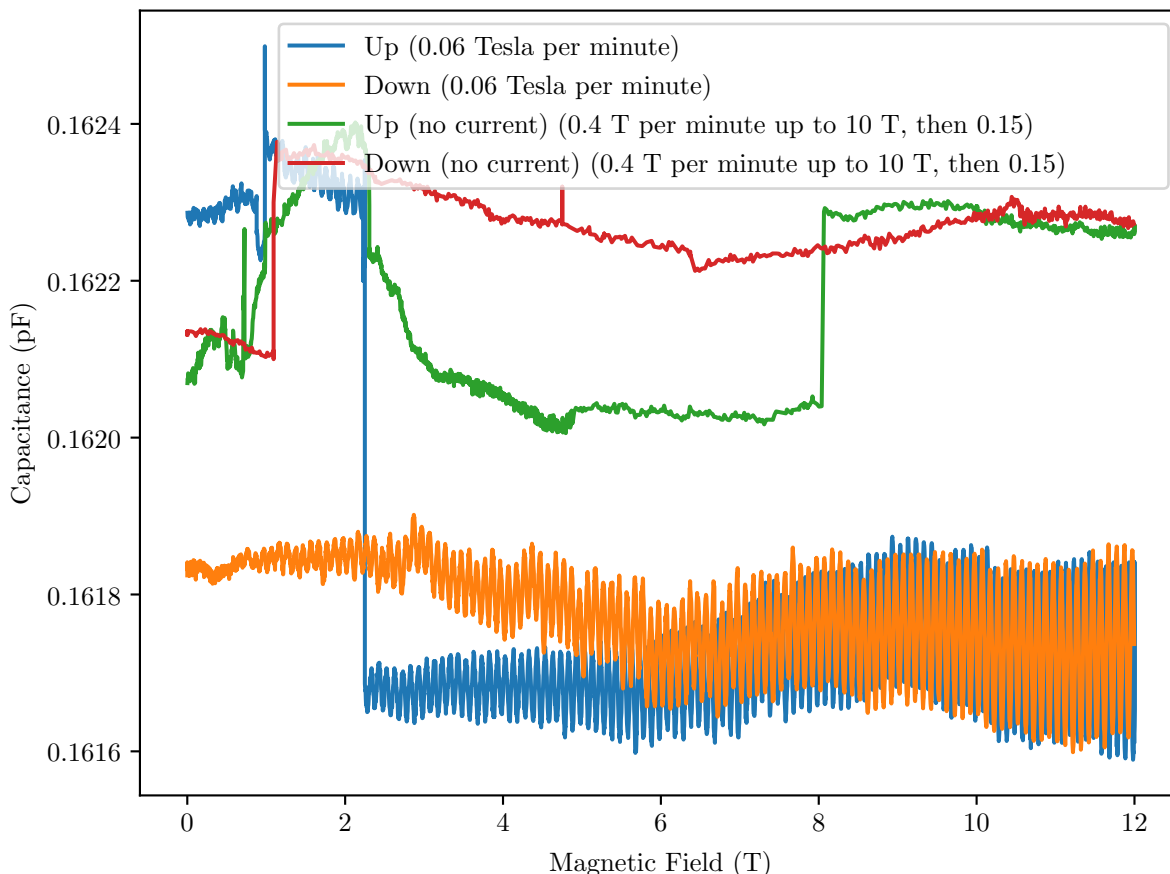


Figure 3.14: Second set of field sweeps of 0.0064 g of InSb, while sending a sinusoidal current of 1 mA at 10 mHz through the coil, at 4.2 K.

4 Oscillating Cantilever Magnetometry

In the previous section we have described torque magnetometry and have characterized our setup at HFML. In this section we will simulate our extended cantilever plus coil setup, and fully describe cantilever magnetometry. Figure 3.15 shows us the basic idea of the setup, note that in the figure the cantilever's oscillation direction is perpendicular to the applied field, while our setup (Figure 3.3a) is rotated 90° and therefore the oscillation direction is parallel to the applied magnetic field. This changes the mathematics of the problem slightly, but the principle stays the same, in our derivations we will always assume our setup and thus that the magnetic field is parallel to the oscillation direction. The cantilever will have a resonant frequency depending on the geometry of the cantilever and the material it is made of. If we now glue a sample on our cantilever and apply a magnetic field to this sample. The magnetic field will exert a force on the magnetized sample, and thus on the cantilever. This force will change the resonant frequency of the cantilever. The change in resonant frequency will be directly dependent on the size of the applied force, and thus on the magnetization of the sample.

We use Newton's second law to find the following differential equation:

$$\frac{d^2z}{dt^2} + 2\zeta\omega_0 \frac{dz}{dt} + \omega_0^2 z = \frac{F_0}{M} \sin(\omega t) + \frac{F_1(z)}{M} \quad (4.1)$$

Here ζ is the damping ratio, ω_0 is the resonant frequency of the cantilever, ω is the frequency at which we drive the oscillation, F_0 is the amplitude of the oscillating force applied with the coil, F_1 is the force applied to the cantilever as a result of the magnetization of the sample, and M is the total mass of the cantilever-coil-sample system. The derivation of the solution to this differential equation can be found in Appendix B, the solution is shortly summarized here:

$$z(t) = A \sin(\omega t + \phi) + B \quad (4.2)$$

Where the amplitude A is given by:

$$A = \frac{F_0}{M \sqrt{\left(\omega^2 - \omega_0^2 + \frac{1}{M} \frac{\partial F_1}{\partial z} \Big|_{z=h} \right)^2 + 4\zeta^2 \omega_0^2 \omega^2}} \quad (4.3)$$

The phase ϕ is given by:

$$\phi = \arctan \left(\frac{2\zeta\omega_0\omega}{\omega^2 - \omega_0^2 + \frac{1}{M} \frac{\partial F_1}{\partial z} \Big|_{z=h}} \right) \quad (4.4)$$

And the offset B is given by:

$$B = \frac{F_1(h) - \frac{\partial F_1}{\partial z} \Big|_{z=h} h}{M\omega_0^2 - \frac{\partial F_1}{\partial z} \Big|_{z=h}} \quad (4.5)$$

Here h is the height above or below the magnetic field centre where are cantilever-coil-sample-system is positioned. From Equation 3.7 we have an expression for the torque exerted by a magnetized sample on the cantilever, we can convert this back to the force by dividing it by $-L_c$:

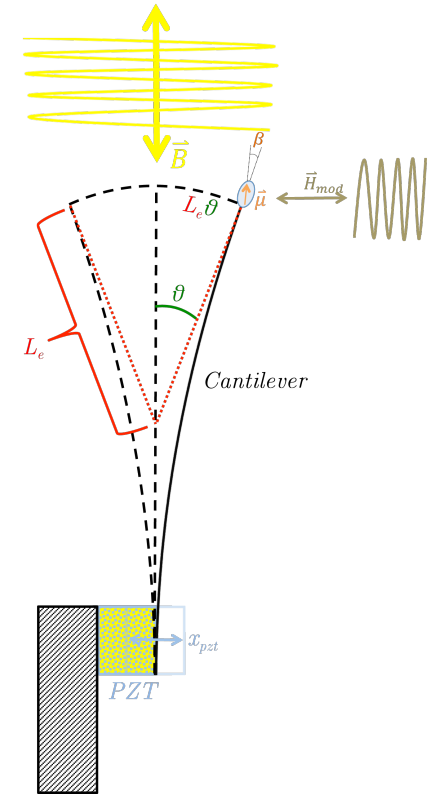


Figure 3.15: Schematic of a oscillating cantilever, the oscillation is driven by the coil on the right. L_e shown here is not accurate for our cantilevers.

$$F = \frac{m_{\perp}}{L_c} B + \frac{\partial(m_{\parallel} B)}{\partial z} = \left(\frac{m_{\perp}}{L_c} + m_{\parallel} \frac{\partial}{\partial z} \right) B \quad (4.6)$$

From this it immediately follows that:

$$\frac{\partial F}{\partial z} = \frac{1}{L_c} \frac{\partial(m_{\perp} B)}{\partial z} + \frac{\partial^2(m_{\parallel} B)}{\partial z^2} = \left(\frac{m_{\perp}}{L_c} + m_{\parallel} \frac{\partial}{\partial z} \right) \frac{\partial B}{\partial z} \quad (4.7)$$

We thus find that the both the amplitude and phase change when a force gradient is applied to the system. In addition, the offset is dependent both on the force gradient, and on the force itself.

Furthermore, the cantilever's resonant frequency can be calculated from the properties of the cantilever, using Equation 4.8:

$$\omega_0 = \sqrt{\frac{k}{\mathcal{M}}} = \sqrt{\frac{vtE}{L_a \mathcal{M}}} \quad (4.8)$$

The force F_1 leads to a shift in this resonant frequency, looking at Equations 4.3 and 4.4 we conclude that the new resonant frequency is given by:

$$\omega_{0_{\text{new}}}^2 = \omega_0^2 - \frac{1}{\mathcal{M}} \frac{\partial F_1}{\partial z} \Big|_{z=h} \quad (4.9)$$

4.1 Simulating Cantilever Magnetometry

Figures 4.1 and 4.4, show us a simulation of Equations 4.3 and 4.4 respectively as a function of the damping parameter ζ and the drive frequency ω . We have used Equation 4.8 for the resonant frequency ω_0 and Equation 3.35 for the temperature dependence of the elastic modulus E . Furthermore, F_1 and $\frac{\partial F_1}{\partial z}$ are given by Equations 4.6 and 4.7 respectively, where the magnetic moment m_{\parallel} in this equation is given by Equation 2.5, and $m_{\perp} = 0$. F_0 is also given by Equation 4.6, with the magnetic moment m_{\parallel} in this equation given by $m = nIA_{\text{coil}}$ and $m_{\perp} = 0$, here n is the number of windings the coil consists of, I is the current sent through the coil, and A_{coil} is the surface area of each winding $A_{\text{coil}} = \pi r_{\text{coil}}^2$. In this simulation, we use the same sample of InSb that we used before in Section 2.2.2. The numerical values used as input can be found in Tables 1 and 2.

L_c	L_a	v	t	r_{coil}	\mathcal{M}	I	E_0
6.25 mm	4.25 mm	0.4 mm	0.080 mm	1.5 mm	0.0390 g	1 mA	155 GPa

Table 2: Input data used for the simulation in Figures 4.1 and 4.4.

4.1.1 Amplitude

We see in both Figures 4.2 and 4.3 that the change in amplitude is just linear with field. This indicates that the effect that the oscillating magnetic moment of the coil has on the cantilever's oscillations dominates the effect of the quantum oscillating magnetic moment of the sample of InSb.

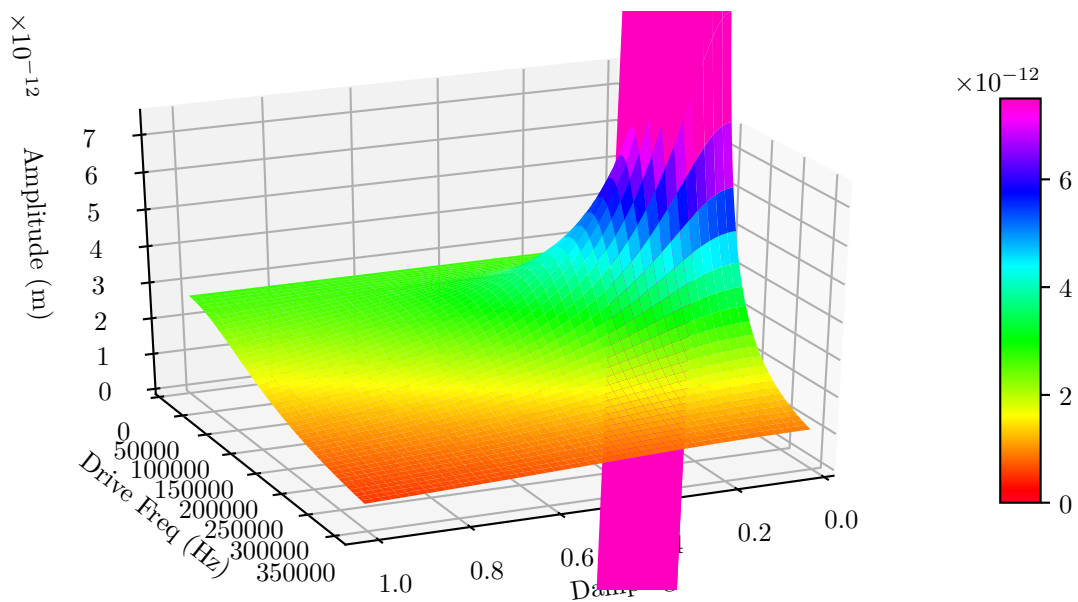


Figure 4.1: Simulation of the amplitude of a driven oscillating cantilever, at 4 K and 10 T 1 cm above the field centre.

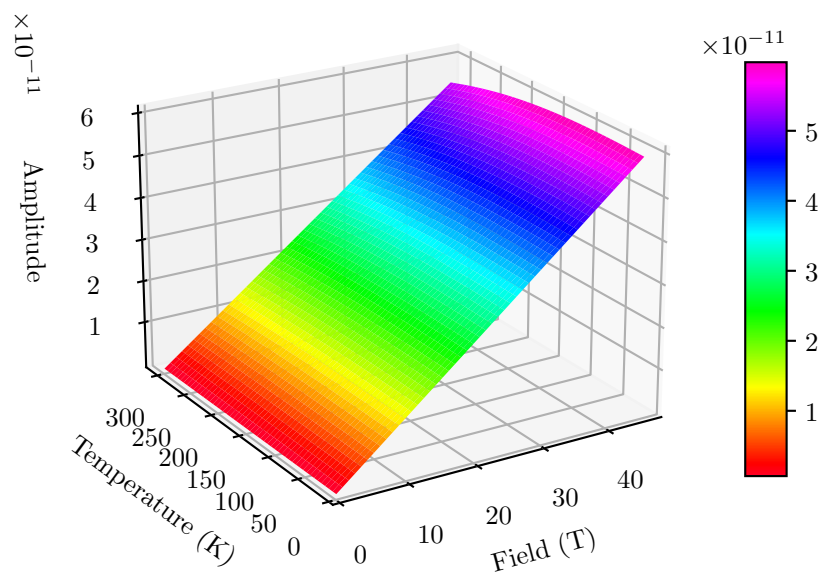


Figure 4.2: Simulation of the amplitude of a driven oscillating cantilever, oscillation is driven with the resonant frequency at 0 K and a damping parameter of 0.1, 1 cm above the field centre.

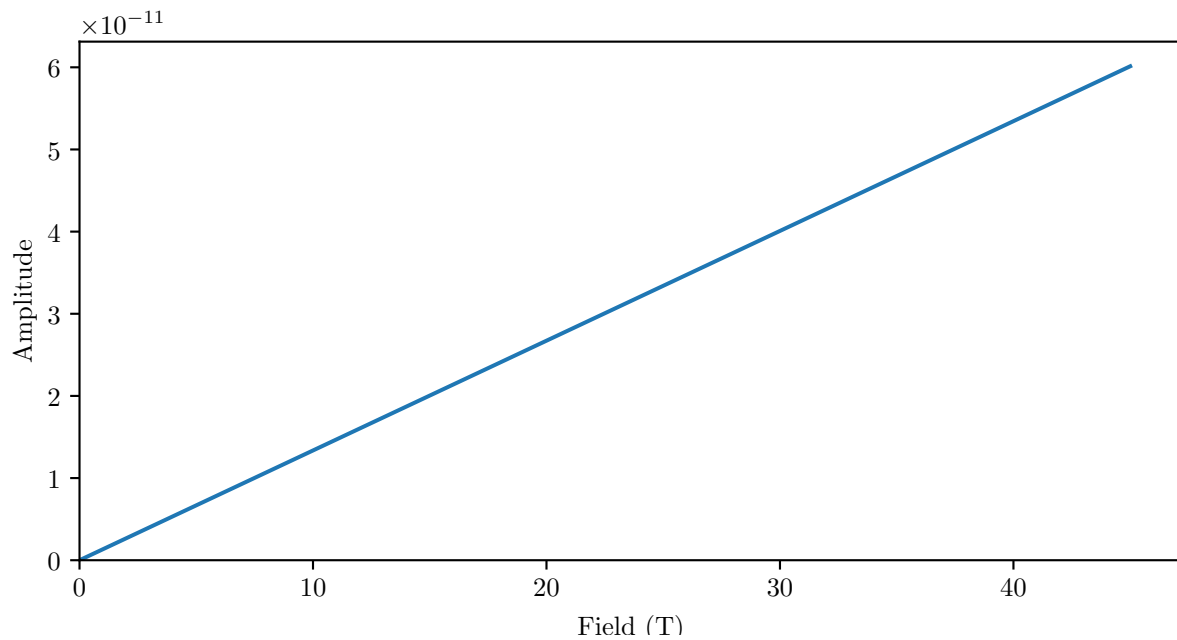


Figure 4.3: Cross-section of Figure 4.2 at 4.2 K.

4.1.2 Phase

In Figure 4.6, on the other hand, we can clearly see the effect of the quantum oscillations on the phase shift between the sinusoidal current input and the resulting sinusoidal oscillations of the cantilever. However, the phase shift appears to be of the order of 1×10^{-10} radians. which is very small. The temperature dependence in Figure 4.5 is due to the temperature dependence of the elasticity of the cantilever as expressed in Equation 3.35.

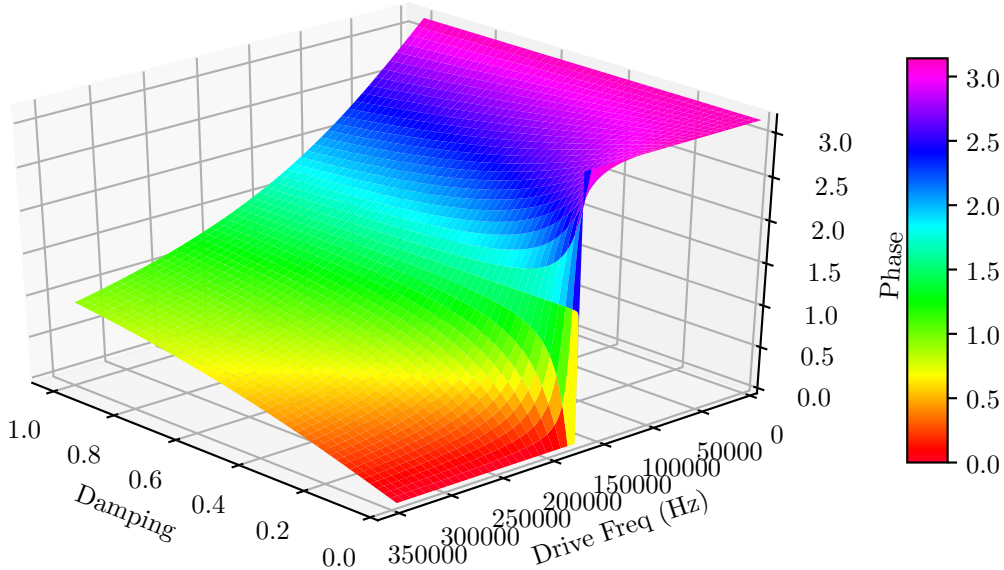


Figure 4.4: Simulation of the phase of a driven oscillating cantilever, at 4K and 10T 1cm above the field centre.

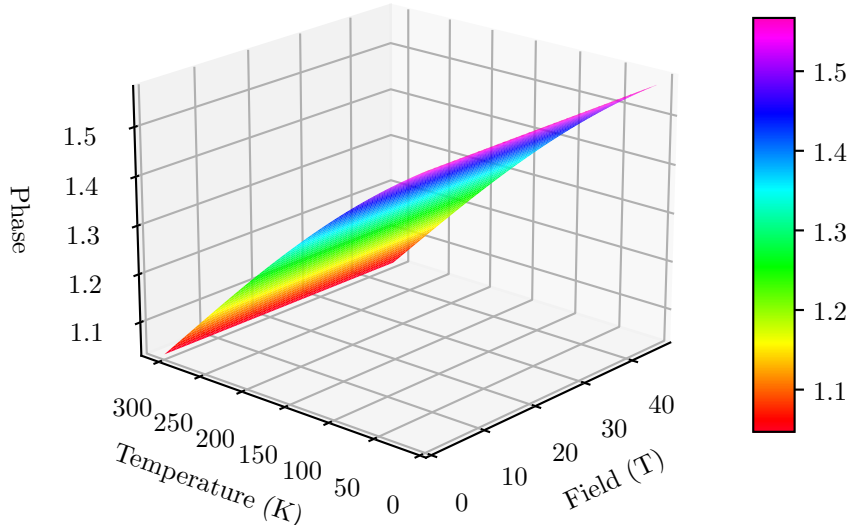


Figure 4.5: Simulation of the phase of a driven oscillating cantilever, oscillation is driven with the resonant frequency at 0K and a damping parameter of 0.1, 1cm above the field centre.

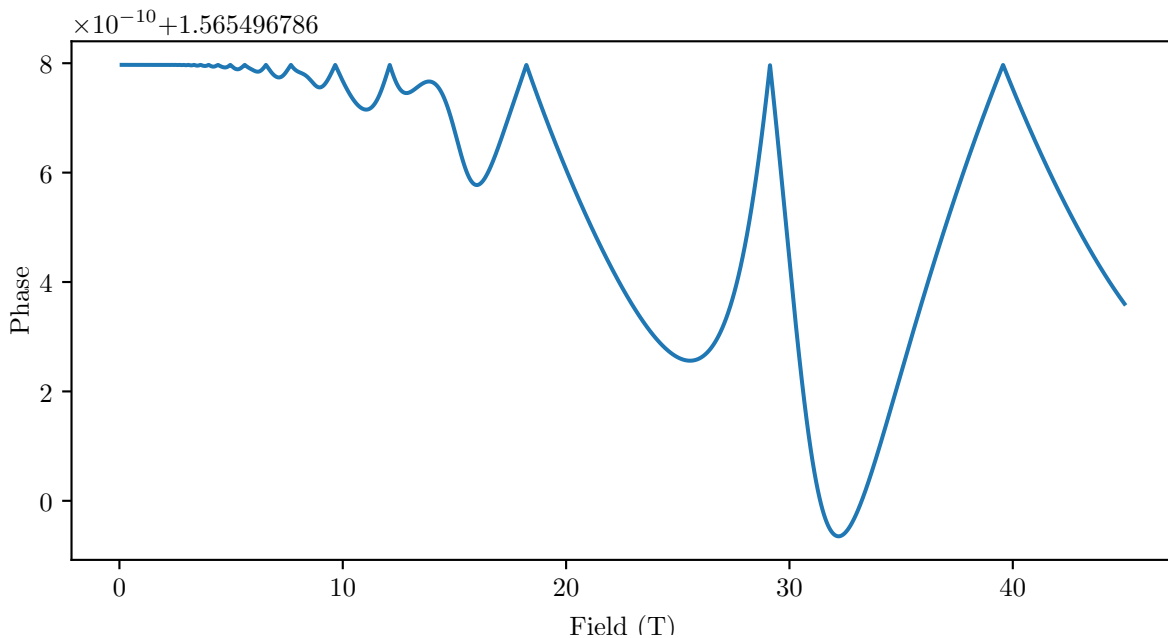


Figure 4.6: Cross-section of Figure 4.5 at 4.2 K.

4.1.3 Resonant Frequency

Figure 4.8 tells us that the quantum oscillations cause a downwards shift in the resonant frequency of a couple of μHz . Once again, the temperature dependence in Figure 4.7 is due to the temperature dependence of the elasticity of the cantilever.

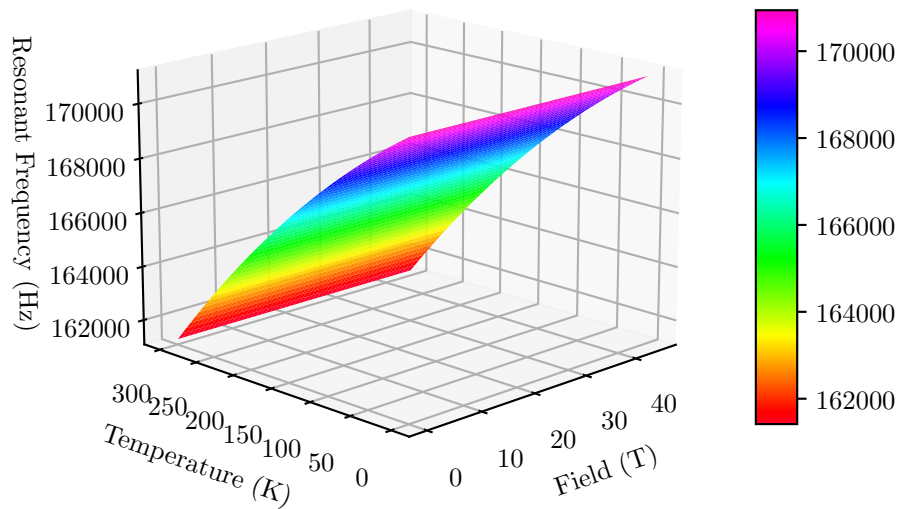


Figure 4.7: Simulation of the resonant frequency of a driven oscillating cantilever, with a damping parameter of 0.1, 1 cm above the field centre.

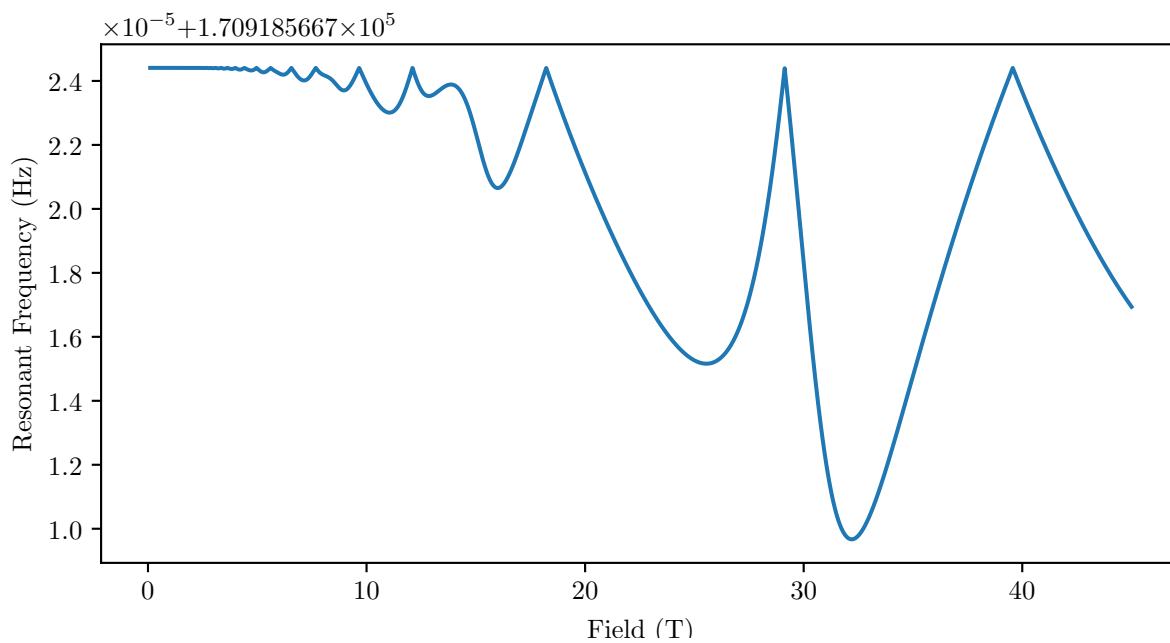


Figure 4.8: Cross-section of Figure 4.7 at 4.2 K.

Thus we find that we cannot resolve the sample's quantum oscillations in the change of amplitude as a function of magnetic field. However, we do find phase shifts of the order 1×10^{-10} as a result of these oscillations. Furthermore, we find that the resonant frequency oscillates with order 1×10^{-5} with respect to the resonant frequency at 0 T which is of the order 1×10^5 . Therefore, once again we find a 1×10^{-10} difference.

5 Conclusion and Discussion

Starting from a (DC) torque magnetometry setup, we have succeeded in extending this setup to create an oscillating cantilever. The oscillations of the cantilever are clearly visible in the oscillating capacitance, both for a large (and thus heavy) coil of a 1000 windings and a smaller coil of merely 50 windings. By varying the current through (and thus the magnetic moment of) the coil we found that the large coil responds with $(1.5 \pm 0.3) \times 10^3 \frac{\text{pF}}{\text{N m}}$ and the small coil with $(8.10 \pm 0.22) \times 10^3 \frac{\text{pF}}{\text{N m}}$. By varying the position in the magnetic field where the cantilever oscillates we found that the large coil responds with $(67 \pm 11) \frac{\text{pF}}{\text{N m}}$, due to excessive noise in the corresponding measurement we were unable to extract this value for the small coil.

By performing field sweeps, we found that the change in amplitude of the oscillations as a function of the magnetic field is dominated by the magnetic moment of the coil, even for the small coil. This leaves us unable to resolve the quantum oscillations in the magnetic moment of the sample. Nonetheless, a transport measurement of the sample does show us quantum oscillations in the conductivity.

As described in Section 3.5 we had some trouble with jumps and drifts during the measurement. These drifts and jumps can have many causes, such as: temperature fluctuations, changes in the grounding and external mechanical vibrations and disturbances. They can be reduced by for example, increasing the thermal conductivity to the anti-cryostat by inserting some Helium gas into the vacuum which should increase the stability of the temperature. However, the drifts and jumps are very difficult to eliminate completely. Likely these jumps and drifts have less effect on a measurement of the phase or (resonant) frequency, compared to the amplitude measurements we have been doing.

We have also had issues with the accuracy of the amplitude versus position measurement of the small coil (Figure 3.9). The errors in the fitted amplitude proved to large to fit a parabola through them. As can be seen in Figure C.3 the measured sinuses are very noisy, and some of them are slightly drifting. Which explains the relatively large error in the fitted amplitude. This is especially problematic for the smaller coil, since it has 20 times less windings and therefore a 20 times smaller magnetic moment, the signal to noise ratio is far worse (Compare Figures C.1 and C.2 with Figures C.3 and C.4).

5.1 Suggestions for further research

The amplitude as a function of field measurements we did in Figures 3.13 and 3.14 were entirely dominated by the magnetic moment of the coil, this result was predicated by our simulations in Figure 4.3. However, this does leave us unable to resolve the quantum oscillations in the magnetic moment. As already hinted at in Section 3.5, a phase sensitive measurement, or a measurement of the shift in resonant frequency, might be able to resolve the oscillations in the magnetic moment of the sample (See Figures 4.6 and 4.8).

In principle, a phase sensitive measurement could be done using a lock-in amplifier and a Wien bridge[5] (the basic circuit component of a capacitance bridge, see Figure 5.1) instead of the Andeen-Hagerling 2700A capacitance bridge. The capacitance C_2 should be chosen to approximately match the capacitance C_x between the cantilever and base plate (e.g. 0.1 pF). When the sinus output is connected to the U_{wy} terminal and to the coil, the capacitance between the cantilever and the base plate C_x will oscillate.

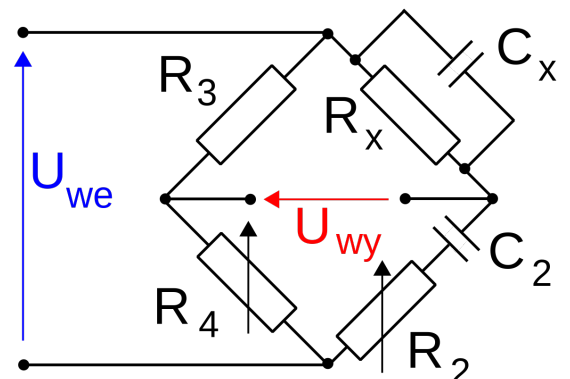


Figure 5.1: Wien bridge circuit

This, should cause the voltage across the U_{we} terminal to oscillate accordingly, which can then be measured by connecting the terminals to the input of the lock-in amplifier. Such an alternate way of measuring the capacitance provides less accuracy in the actual value of the capacitance compared to the Andeen-Hagerling capacitance bridge, as we now measure voltage instead of capacitance. However, it does enable us to do the measurement phase sensitively.

A potential pitfall in measuring the phase shift is that the phase shift is very small (of the order of 1×10^{-10} , see Figure 4.6), and therefore a very large accuracy is required. If such a measurement would therefore prove unfeasible, a potential workaround might be to measure the shift in resonant frequency instead. To accomplish this a similar setup could be used. However, now the amplitude versus frequency has to be determined, and from that the resonant frequency, at a specific magnetic field.

Furthermore, to very precisely measure the amplitude of the cantilever's oscillations, it might be possible to use a pulsed laser whose frequency is either the same as the drive frequency or double the drive frequency, and 90° phase shifted with respect to the drive frequency. The laser would hit the cantilever precisely when its oscillations are at a maximum or a minimum and reflect back, the time this takes is directly proportional to the amplitude of the oscillation. This might make scanning over a frequency range and finding the maximum amplitude, and thus the resonant frequency, relatively easy and fast.

6 Acknowledgements and References

First of all, massive thanks to Uli Zeitler, for making this all possible, and answering all my many questions. Thanks also to Maurice Bal, who helped me a lot with the actual measurements. Because of the Covid-19 pandemic the time for experiments in the laboratory was limited, Uli and Maurice helped me spend the many hours at home during the lock-down productively working on a simulation of the experiments, whose results now constitute a major part of this thesis, thanks to both of them for answering my many emails. Also, a big Thank You to the rest of the Staff and Students at HFML, who were very helpful and showed me how to use all the equipment and tools that I was unfamiliar with.

References

- [1] T. van Wolfswinkel. "De Haas van Alphen effect in InSb". MA thesis. Nijmegen: High Field Magnet Laboratory, June 2019, p. 27.
- [2] D. Zakarian, A. Khachatrian, and S. Firstov. "Universal temperature dependence of Young's modulus". In: *Metal Powder Report* 74.4 (2019), pp. 204–206. ISSN: 0026-0657.
- [3] *HFML magnet specifications*. URL: <https://www.ru.nl/hfml/facility/experimental/magnets/>.
- [4] L. Peters. "High-field cantilever magnetometry". MA thesis. Nijmegen: High Field Magnet Laboratory, Sept. 2017. Chap. 2.
- [5] P. Horowitz and W. Hill. *The Art of Electronics*. 3rd ed. Cambridge University Press, 2016. Chap. 7.1.5.B, pp. 436–438. ISBN: 9780521809269.
- [6] R. A. Serway and J. W. Jewett Jr. *Physics for Scientists and Engineers, Technology Update*. 9th ed. Cengage Learning, Jan. 2015. Chap. 29.6. ISBN: 9781305401969.
- [7] C. Kittel. *Introduction to Solid State Physics*. 8th ed. Wiley, Nov. 2004. Chap. 11,12. ISBN: 9780471415268.
- [8] U. Zeitler. "Magneto-Transport in Semiconductors at low Temperatures and high Magnetic Fields". PhD thesis. Grenoble High Magnetic Field Laboratory, 1994.
- [9] O. Madelung, ed. *Semiconductors: Group IV Elements and III-V Compounds*. 1st ed. Data in Science and Technology. Springer-Verlag, 1991. Chap. 2.15, pp. 141–149. ISBN: 9783540531500.
- [10] A. A. Abrikosov. *Fundamentals of the theory of metals*. Trans. by A. Beknazarov. Elsevier Science Publishers, 1988. ISBN: 0444870946.
- [11] D. Shoenberg. *Magnetic Oscillations in Metals*. Cambridge Monographs on Physics. Cambridge: Cambridge University Press, 1984. ISBN: 9780511897870.

A Integral Solution

Here we will solve:

$$C_1 = \int_{L_c-r}^{L_c+r} \frac{\epsilon_0 2 \sqrt{r^2 - (x - L_c)^2}}{d_0 - \frac{FL_a^2}{2EI}x + \frac{FL_a^3}{6EI}} dx$$

We start by doing a coordinate transformation $\alpha = x - L_c$ to the centre of the capacitive plate:

$$\begin{aligned} C_1 &= \int_{-r}^r \frac{2\epsilon_0 \sqrt{r^2 - \alpha^2}}{d_0 - \frac{FL_a^2}{2EI}(\alpha + L_c) + \frac{FL_a^3}{6EI}} d\alpha \\ &\Rightarrow \int_{-r}^r \frac{2\epsilon_0 \sqrt{r^2 - \alpha^2}}{d_0 - \frac{FL_a^2}{2EI}\alpha + \frac{FL_a^2}{6EI}(L_a - 3L_c)} d\alpha \end{aligned}$$

We use that $L_c = L_a + r$ to reduce the amount of variables:

$$\begin{aligned} C_1 &= \int_{-r}^r \frac{2\epsilon_0 \sqrt{r^2 - \alpha^2}}{d_0 - \frac{FL_a^2}{2EI}\alpha + \frac{FL_a^2}{6EI}(-2L_a - 3r)} d\alpha \\ &\Rightarrow \int_{-r}^r \frac{2\epsilon_0 \sqrt{r^2 - \alpha^2}}{d_0 - \frac{FL_a^2}{2EI}\alpha - \frac{FL_a^3}{3EI} - \frac{FL_a^2 r}{2EI}} d\alpha \\ &\Rightarrow \frac{2\epsilon_0 EI}{FL_a^2} \int_{-r}^r \frac{\sqrt{r^2 - \alpha^2}}{\frac{d_0 EI}{FL_a^2} - \alpha/2 - L_a/3 - r/2} d\alpha \\ &\Rightarrow \frac{12\epsilon_0 EI}{FL_a^2} \int_{-r}^r \frac{\sqrt{r^2 - \alpha^2}}{\frac{6d_0 EI}{FL_a^2} - 3\alpha - 2L_a - 3r} d\alpha \\ &\Rightarrow \frac{12\epsilon_0 EI}{FL_a^2} \int_{-r}^r \frac{\sqrt{r^2 - \alpha^2}}{\frac{6d_0 EI}{FL_a^2} - 3(r + \alpha) - 2L_a} d\alpha \end{aligned}$$

Now we switch to polar coordinates $\alpha = r \cos(\phi)$, $d\alpha = -r \sin(\phi)d\phi$, $\sqrt{r^2 - \alpha^2} = r \sin(\phi)$:

$$\begin{aligned} C_1 &= \frac{-12\epsilon_0 EI}{FL_a^2} \int_{\pi}^0 \frac{r \sin(\phi)}{\frac{6d_0 EI}{FL_a^2} - 3r(1 + \cos(\phi)) - 2L_a} r \sin(\phi) d\phi \\ &\Rightarrow \frac{12\epsilon_0 EI}{FL_a^2} \int_0^{\pi} \frac{r^2 \sin(\phi)^2}{\frac{6d_0 EI}{FL_a^2} - 3r(1 + \cos(\phi)) - 2L_a} d\phi \end{aligned}$$

Next we do a transformation that might not be completely obvious but it will prove helpful: $u = \tan(\phi/2)$, $du = 1/\left(2 \cos(\phi/2)^2\right) d\phi$

$$\begin{aligned} u &= \tan(\phi/2) = \frac{\sin(\phi/2)}{\cos(\phi/2)} = \frac{\sin(\phi)}{2 \cos(\phi/2)^2} = \frac{\sin(\phi)}{1 + \cos(\phi)} \\ \Rightarrow \sin(\phi) &= u 2 \cos(\phi/2)^2 = \frac{2u \cos(\phi/2)^2}{\sin(\phi/2)^2 + \cos(\phi/2)^2} = \frac{2u}{\frac{\sin(\phi/2)^2}{\cos(\phi/2)^2} + 1} = \frac{2u}{\tan(\phi/2)^2 + 1} = \frac{2u}{u^2 + 1} \\ \Rightarrow 1 + \cos(\phi) &= \frac{\sin(\phi)}{u} = \frac{2}{u^2 + 1} \\ \Rightarrow \cos(\phi) &= \frac{2}{u^2 + 1} - 1 = \frac{2}{u^2 + 1} - \frac{u^2 + 1}{u^2 + 1} = \frac{1 - u^2}{1 + u^2} \end{aligned}$$

$$\implies d\phi = 2du \cos(\phi/2)^2 = 2du \frac{\sin(\phi)}{2u} = \frac{2du}{1+u^2}$$

Plugging all this in gives:

$$\begin{aligned} C_1 &= \frac{12\epsilon_0 EI}{FL_a^2} \int_0^\infty \frac{r^2 \frac{4u^2}{(1+u^2)^2}}{\frac{6d_0 EI}{FL_a^2} - 3r \left(\frac{2}{1+u^2} \right) - 2L_a} \frac{2du}{1+u^2} \\ &\implies \frac{12\epsilon_0 EI}{FL_a^2} \int_0^\infty \frac{8r^2 u^2}{\frac{6d_0 EI}{FL_a^2} - \frac{6r}{1+u^2} - 2L_a} \frac{du}{(1+u^2)^3} \\ &\implies \frac{12\epsilon_0 EI}{FL_a^2} \int_0^\infty \frac{8r^2 u^2}{\left(\frac{6d_0 EI}{FL_a^2} - 2L_a \right) (1+u^2) - 6r} \frac{du}{(1+u^2)^2} \\ &\implies \frac{16\epsilon_0 EIr}{FL_a^2} \int_0^\infty \underbrace{\frac{u^2}{\left(\frac{d_0 EI}{rFL_a^2} - \frac{L_a}{3r} \right) (1+u^2)^3 - (1+u^2)^2}}_c du \\ &\implies \frac{16\epsilon_0 EIr}{FL_a^2} \int_0^\infty \frac{1}{(1+u^2)^2} \frac{u^2}{c(1+u^2)-1} du \\ &\implies \frac{16\epsilon_0 EIr}{FL_a^2} \int_0^\infty \frac{1}{(1+u^2)^2} \frac{u^2}{cu^2+c-1} du \\ &\implies \frac{16\epsilon_0 EIr}{FL_a^2} \int_0^\infty \frac{c-1}{u^2+1} - \frac{c(c-1)}{cu^2+c-1} + \frac{1}{(1+u^2)^2} du \\ &\implies \frac{16\epsilon_0 EIr}{FL_a^2} \left((c-1) [\arctan(u)]_0^\infty - \int_0^\infty \frac{c(c-1)}{(c-1) \left(\frac{cu^2}{c-1} + 1 \right)} du + \int_0^\infty \frac{1}{(1+u^2)^2} du \right) \end{aligned}$$

In the last integral we substitute $u = \tan(s)$, $du = 1/\cos(s)^2 ds$:

$$C_1 = \frac{16\epsilon_0 EIr}{FL_a^2} \left((c-1) \frac{\pi}{2} - \int_0^\infty \frac{c}{\frac{cu^2}{c-1} + 1} du + \int_0^{\pi/2} \frac{1}{\left(1 + \tan(s)^2 \right)^2} \frac{ds}{\cos(s)^2} \right)$$

In the middle term we substitute $t = \sqrt{\frac{c}{c-1}}u$, $dt = \sqrt{\frac{c}{c-1}}du$

$$\begin{aligned} C_1 &= \frac{16\epsilon_0 EIr}{FL_a^2} \left((c-1) \frac{\pi}{2} - c \sqrt{\frac{c-1}{c}} \int_0^\infty \frac{1}{t^2+1} dt + \int_0^{\pi/2} \frac{1}{\left(\frac{\cos(s)^2}{\cos(s)^2} + \frac{\sin(s)^2}{\cos(s)^2} \right)^2} \frac{ds}{\cos(s)^2} \right) \\ &\implies \frac{16\epsilon_0 EIr}{FL_a^2} \left((c-1) \frac{\pi}{2} - \sqrt{c(c-1)} [\arctan(t)]_0^\infty + \int_0^{\pi/2} \cos(s)^2 ds \right) \\ &\implies \frac{16\epsilon_0 EIr}{FL_a^2} \left((c-1) \frac{\pi}{2} - \sqrt{c(c-1)} \frac{\pi}{2} + \int_0^{\pi/2} \frac{1}{2} + \frac{\cos(2s)}{2} ds \right) \\ &\implies \frac{16\epsilon_0 EIr}{FL_a^2} \left((c-1) \frac{\pi}{2} - \sqrt{c(c-1)} \frac{\pi}{2} + \frac{\pi}{4} + \left[\frac{\sin(2s)}{2} \right]_0^{\pi/2} \right) \\ &\implies \frac{8\pi\epsilon_0 EIr}{FL_a^2} \left(c-1 - \sqrt{c(c-1)} + \frac{1}{2} \right) \end{aligned}$$

$$\Rightarrow \frac{8\pi\epsilon_0 EI r}{FL_a^2} \left(c - \frac{1}{2} - \sqrt{c(c-1)} \right)$$

$$C_1 = \frac{8\pi\epsilon_0 EI r}{FL_a^2} \left(\frac{d_0 EI}{r FL_a^2} - \frac{L_a}{3r} - \frac{1}{2} - \sqrt{\left(\frac{d_0 EI}{r FL_a^2} - \frac{L_a}{3r} \right) \left(\frac{d_0 EI}{r FL_a^2} - \frac{L_a}{3r} - 1 \right)} \right)$$

(A.1)

We can simplify Equation A.1 a bit by performing a Taylor expansion on the square root:

$$\begin{aligned} C_1 &= \frac{8\pi\epsilon_0 EI r}{FL_a^2} \left(c - \frac{1}{2} - \sqrt{c(c-1)} \right) = \frac{8\pi\epsilon_0 EI r}{FL_a^2} \left(c - \frac{1}{2} - c\sqrt{1 - \frac{1}{c}} \right) \\ \Rightarrow &\frac{8\pi\epsilon_0 EI r c}{FL_a^2} \left(1 - \frac{1}{2c} - \sqrt{1 - \frac{1}{c}} \right) \approx \frac{8\pi\epsilon_0 EI r c}{FL_a^2} \left(1 - \frac{1}{2c} - \left(1 - \frac{1}{2c} - \frac{1}{8c^2} + \mathcal{O}(c^{-3}) \right) \right) \\ \Rightarrow &\frac{8\pi\epsilon_0 EI r c}{FL_a^2} \frac{1}{8c^2} = \frac{\pi\epsilon_0 EI r}{FL_a^2 c} = \frac{\pi\epsilon_0 EI r}{FL_a^2 \left(\frac{d_0 EI}{r FL_a^2} - \frac{L_a}{3r} \right)} = \frac{\epsilon_0 EI \overbrace{\pi r^2}^A}{d_0 EI - \frac{FL_a^3}{3}} \\ C_1 &= \frac{\epsilon_0 A}{d_0 - \frac{FL_a^3}{3EI}} \end{aligned}$$
(A.2)

B Differential Equation Solution

Here we will try to find the solution of:

$$\frac{d^2z}{dt^2} + 2\zeta\omega_0 \frac{dz}{dt} + \omega_0^2 z = \frac{F_0}{M} \sin(\omega t) + \frac{F_1(z)}{M}$$

We start with the following ansatz for the solution:

$$z(t) = A \sin(\omega t + \phi) + B$$

Using this ansatz we find that:

$$\frac{dz(t)}{dt} = A\omega \cos(\omega t + \phi)$$

And:

$$\frac{d^2z(t)}{dt^2} = -A\omega^2 \sin(\omega t + \phi)$$

We also write $F_1(z)$ as its Taylor expansion:

$$F_1(z) \approx F_1(h) + \left. \frac{\partial F_1}{\partial z} \right|_{z=h} (z - h) + \mathcal{O}(z^2)$$

Where h is the height of our cantilever above or below the field centre ($z = 0$). Plugging all this in gives:

$$\begin{aligned} -A\omega^2 \sin(\omega t + \phi) + 2\zeta\omega_0 A\omega \cos(\omega t + \phi) + \omega_0^2 (A \sin(\omega t + \phi) + B) = \\ \frac{F_0}{M} \sin(\omega t) + \frac{F_1(h)}{M} + \left. \frac{1}{M} \frac{\partial F_1}{\partial z} \right|_{z=h} (A \sin(\omega t + \phi) + B - h) \end{aligned}$$

Collecting all the terms:

$$\begin{aligned} A \sin(\omega t + \phi) \left[\omega_0^2 - \omega^2 - \left. \frac{1}{M} \frac{\partial F_1}{\partial z} \right|_{z=h} \right] + 2\zeta\omega_0 A \cos(\omega t + \phi) + B \left[\omega_0^2 - \left. \frac{1}{M} \frac{\partial F_1}{\partial z} \right|_{z=h} \right] = \\ \frac{F_0}{M} \sin(\omega t) + \frac{F_1(h)}{M} - \left. \frac{1}{M} \frac{\partial F_1}{\partial z} \right|_{z=h} h \end{aligned}$$

Next we use the angle-sum-and-difference formula's on the sine and cosine:

$$\begin{aligned} A (\sin(\omega t) \cos(\phi) + \cos(\omega t) \sin(\phi)) \left[\omega_0^2 - \omega^2 - \left. \frac{1}{M} \frac{\partial F_1}{\partial z} \right|_{z=h} \right] + 2\zeta\omega_0 A (\cos(\omega t) \cos(\phi) - \sin(\omega t) \sin(\phi)) + \\ B \left[\omega_0^2 - \left. \frac{1}{M} \frac{\partial F_1}{\partial z} \right|_{z=h} \right] = \frac{F_0}{M} \sin(\omega t) + \frac{F_1(h)}{M} - \left. \frac{1}{M} \frac{\partial F_1}{\partial z} \right|_{z=h} h \end{aligned}$$

Collecting all the terms again:

$$\begin{aligned} \sin(\omega t) & \left[A \cos(\phi) \left(\omega_0^2 - \omega^2 - \frac{1}{\mathcal{M}} \frac{\partial F_1}{\partial z} \Big|_{z=h} \right) - \frac{F_0}{\mathcal{M}} - 2\zeta\omega_0\omega A \sin(\phi) \right] + \\ & \cos(\omega t) \left[A \sin(\phi) \left(\omega_0^2 - \omega^2 - \frac{1}{\mathcal{M}} \frac{\partial F_1}{\partial z} \Big|_{z=h} \right) + 2\zeta\omega_0\omega A \cos(\phi) \right] + \\ & B \left[\omega_0^2 - \frac{1}{\mathcal{M}} \frac{\partial F_1}{\partial z} \Big|_{z=h} \right] = \frac{F_1(h)}{\mathcal{M}} - \frac{1}{\mathcal{M}} \frac{\partial F_1}{\partial z} \Big|_{z=h} h \end{aligned}$$

This leads to the following three equations:

$$A \cos(\phi) \left(\omega_0^2 - \omega^2 - \frac{1}{\mathcal{M}} \frac{\partial F_1}{\partial z} \Big|_{z=h} \right) - \frac{F_0}{\mathcal{M}} - 2\zeta\omega_0\omega A \sin(\phi) = 0$$

And:

$$A \sin(\phi) \left(\omega_0^2 - \omega^2 - \frac{1}{\mathcal{M}} \frac{\partial F_1}{\partial z} \Big|_{z=h} \right) + 2\zeta\omega_0\omega A \cos(\phi) = 0$$

And:

$$B \left[\omega_0^2 - \frac{1}{\mathcal{M}} \frac{\partial F_1}{\partial z} \Big|_{z=h} \right] = \frac{F_1(h)}{\mathcal{M}} - \frac{1}{\mathcal{M}} \frac{\partial F_1}{\partial z} \Big|_{z=h} h$$

The third equation immediately gives us a result for B :

$$B = \frac{F_1(h) - \frac{\partial F_1}{\partial z} \Big|_{z=h} h}{\mathcal{M}\omega_0^2 - \frac{\partial F_1}{\partial z} \Big|_{z=h}} \quad (\text{B.1})$$

The second equation gives us a result for ϕ :

$$\sin(\phi) \left(\omega_0^2 - \omega^2 - \frac{1}{\mathcal{M}} \frac{\partial F_1}{\partial z} \Big|_{z=h} \right) = -2\zeta\omega_0\omega \cos(\phi)$$

$$\tan(\phi) \left(\omega^2 - \omega_0^2 + \frac{1}{\mathcal{M}} \frac{\partial F_1}{\partial z} \Big|_{z=h} \right) = 2\zeta\omega_0\omega$$

$$\tan(\phi) = \frac{2\zeta\omega_0\omega}{\omega^2 - \omega_0^2 + \frac{1}{\mathcal{M}} \frac{\partial F_1}{\partial z} \Big|_{z=h}} \quad (\text{B.2})$$

Rewriting the first equation leads to a result for A :

$$\begin{aligned} A \left(\cos(\phi) \left(\omega_0^2 - \omega^2 - \frac{1}{\mathcal{M}} \frac{\partial F_1}{\partial z} \Big|_{z=h} \right) - 2\zeta\omega_0\omega \sin(\phi) \right) &= \frac{F_0}{\mathcal{M}} \\ A \cos(\phi) \left(\omega_0^2 - \omega^2 - \frac{1}{\mathcal{M}} \frac{\partial F_1}{\partial z} \Big|_{z=h} - 2\zeta\omega_0\omega \tan(\phi) \right) &= \frac{F_0}{\mathcal{M}} \\ A \frac{\cos(\phi)}{\sqrt{\cos(\phi)^2 + \sin(\phi)^2}} \left(\omega_0^2 - \omega^2 - \frac{1}{\mathcal{M}} \frac{\partial F_1}{\partial z} \Big|_{z=h} - 2\zeta\omega_0\omega \tan(\phi) \right) &= \frac{F_0}{\mathcal{M}} \\ A \frac{1}{\sqrt{1 + \tan(\phi)^2}} \left(\omega_0^2 - \omega^2 - \frac{1}{\mathcal{M}} \frac{\partial F_1}{\partial z} \Big|_{z=h} - 2\zeta\omega_0\omega \tan(\phi) \right) &= \frac{F_0}{\mathcal{M}} \end{aligned}$$

Substituting $\tan(\phi)$ from Equation B.2:

$$\begin{aligned}
A \frac{1}{\sqrt{1 + \left(\frac{2\zeta\omega_0\omega}{\omega^2 - \omega_0^2 + \frac{1}{\mathcal{M}} \frac{\partial F_1}{\partial z} \Big|_{z=h}} \right)^2}} \left(\omega_0^2 - \omega^2 - \frac{1}{\mathcal{M}} \frac{\partial F_1}{\partial z} \Big|_{z=h} - 2\zeta\omega_0\omega \frac{2\zeta\omega_0\omega}{\omega^2 - \omega_0^2 + \frac{1}{\mathcal{M}} \frac{\partial F_1}{\partial z} \Big|_{z=h}} \right) &= \frac{F_0}{\mathcal{M}} \\
A \frac{\omega_0^2 - \omega^2 - \frac{1}{\mathcal{M}} \frac{\partial F_1}{\partial z} \Big|_{z=h}}{\sqrt{(\omega_0^2 - \omega^2 - \frac{1}{\mathcal{M}} \frac{\partial F_1}{\partial z} \Big|_{z=h})^2 + 4\zeta^2\omega_0^2\omega^2}} \left(\omega_0^2 - \omega^2 - \frac{1}{\mathcal{M}} \frac{\partial F_1}{\partial z} \Big|_{z=h} + \frac{4\zeta^2\omega_0^2\omega^2}{\omega_0^2 - \omega^2 - \frac{1}{\mathcal{M}} \frac{\partial F_1}{\partial z} \Big|_{z=h}} \right) &= \frac{F_0}{\mathcal{M}} \\
A \frac{1}{\sqrt{(\omega_0^2 - \omega^2 - \frac{1}{\mathcal{M}} \frac{\partial F_1}{\partial z} \Big|_{z=h})^2 + 4\zeta^2\omega_0^2\omega^2}} \left(\left(\omega_0^2 - \omega^2 - \frac{1}{\mathcal{M}} \frac{\partial F_1}{\partial z} \Big|_{z=h} \right)^2 + 4\zeta^2\omega_0^2\omega^2 \right) &= \frac{F_0}{\mathcal{M}} \\
A \sqrt{\left(\omega_0^2 - \omega^2 - \frac{1}{\mathcal{M}} \frac{\partial F_1}{\partial z} \Big|_{z=h} \right)^2 + 4\zeta^2\omega_0^2\omega^2} &= \frac{F_0}{\mathcal{M}}
\end{aligned}$$

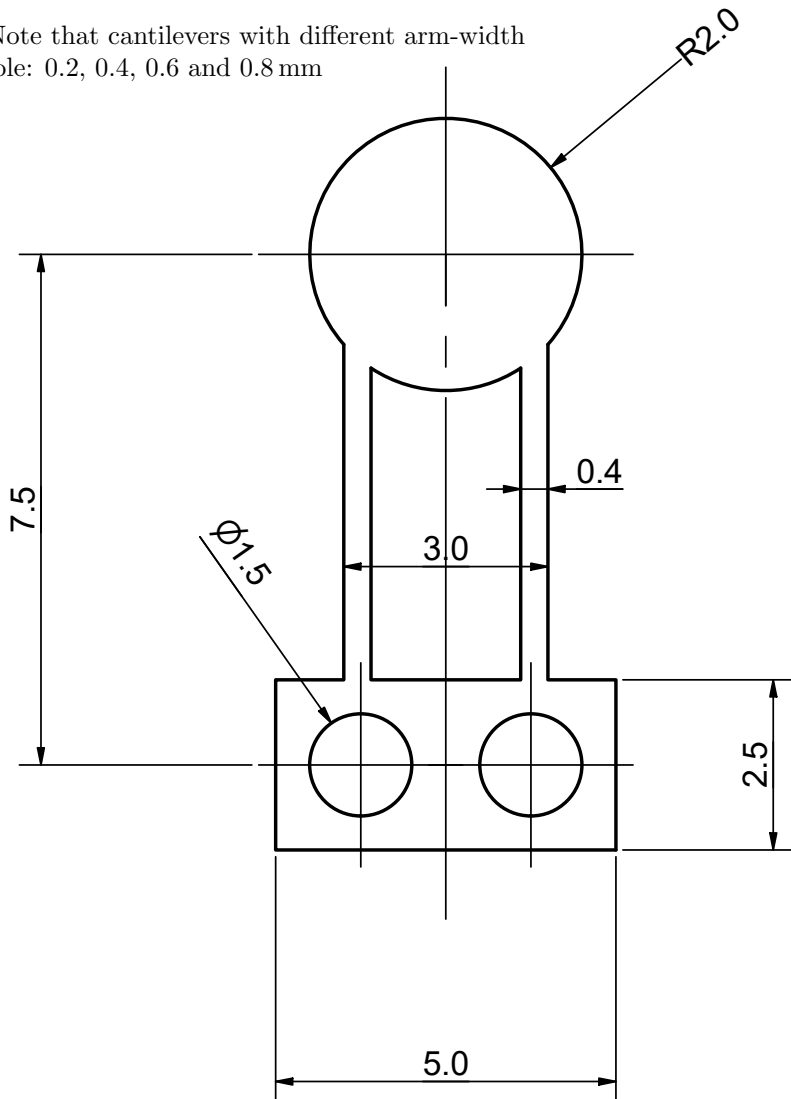
$$A = \frac{F_0}{\mathcal{M} \sqrt{(\omega^2 - \omega_0^2 + \frac{1}{\mathcal{M}} \frac{\partial F_1}{\partial z} \Big|_{z=h})^2 + 4\zeta^2\omega_0^2\omega^2}}$$

(B.3)

C Cantilever Specifications and Oscillation Data

Cantilever [4]	Chemical composition (mass percent)	Thickness	Elastic modulus	Yield strength
Copper beryllium alloy C17410 HT	CuCo _{0.35–0.60} Be _{0.5}	(0.080 ± 0.005) mm	138 GPa	690 to 830 MPa
Copper beryllium alloy C17200 HT	Cu((NiCo) _{min:0.2} Fe) _{max:0.6} Be _{1.80–2.00}	unknown	131 GPa	1130 to 1420 MPa
Phosphor Bronze	CuSn _{5.5–7.0} P _{0.01–0.4}	0.05 and 0.1 mm	118 GPa	300 to 690 MPa
Brass	CuZn _{35.5} Pb _{2.5–3.7}	unknown	100 to 125 GPa	124 to 310 MPa

Table 3: Note that cantilevers with different arm-width are available: 0.2, 0.4, 0.6 and 0.8 mm



Tolerances unless otherwise specified according to NEN-ISO 2768-fK		General Roughness Ra 1.6
Description	Material:	
cantilever-longleg 0.4	Phosphor Bronze	
HFML High Field Magnet Laboratory FNWI Radboud University Nijmegen the Netherlands tel: +31 243652087 www.ru.nl/hfml	Drawn Lijnis	Drawing nr.
	Date 31-Oct-19	
	NB. The copyright/ownership of this drawing is and will remain ours. The drawing must not be copied or used without our authorization or brought to the knowledge of a third party.	Sheet 1 of 1 Revision Format
		No Fixed Scale A4

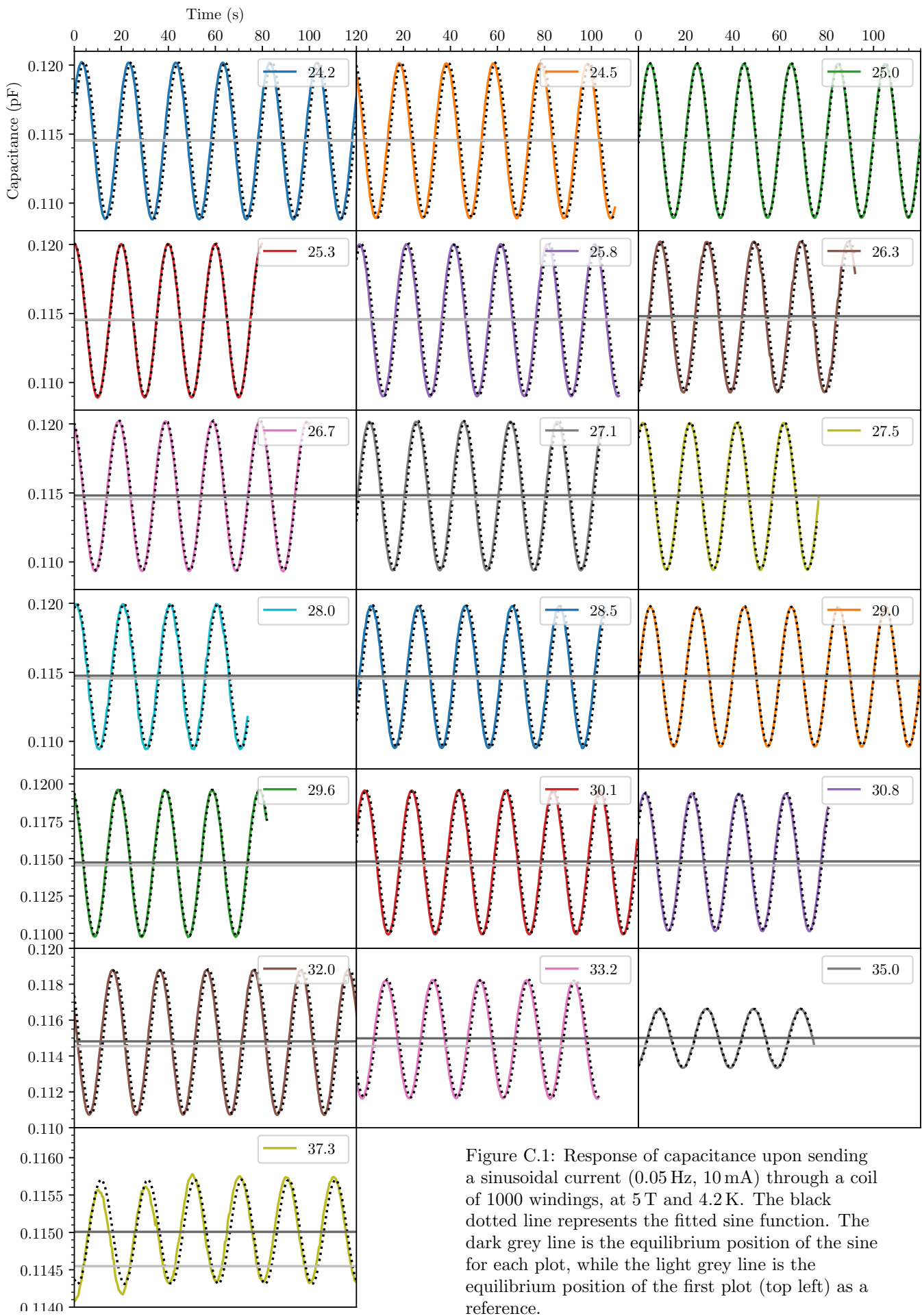


Figure C.1: Response of capacitance upon sending a sinusoidal current (0.05 Hz, 10 mA) through a coil of 1000 windings, at 5 T and 4.2 K. The black dotted line represents the fitted sine function. The dark grey line is the equilibrium position of the sine for each plot, while the light grey line is the equilibrium position of the first plot (top left) as a reference.

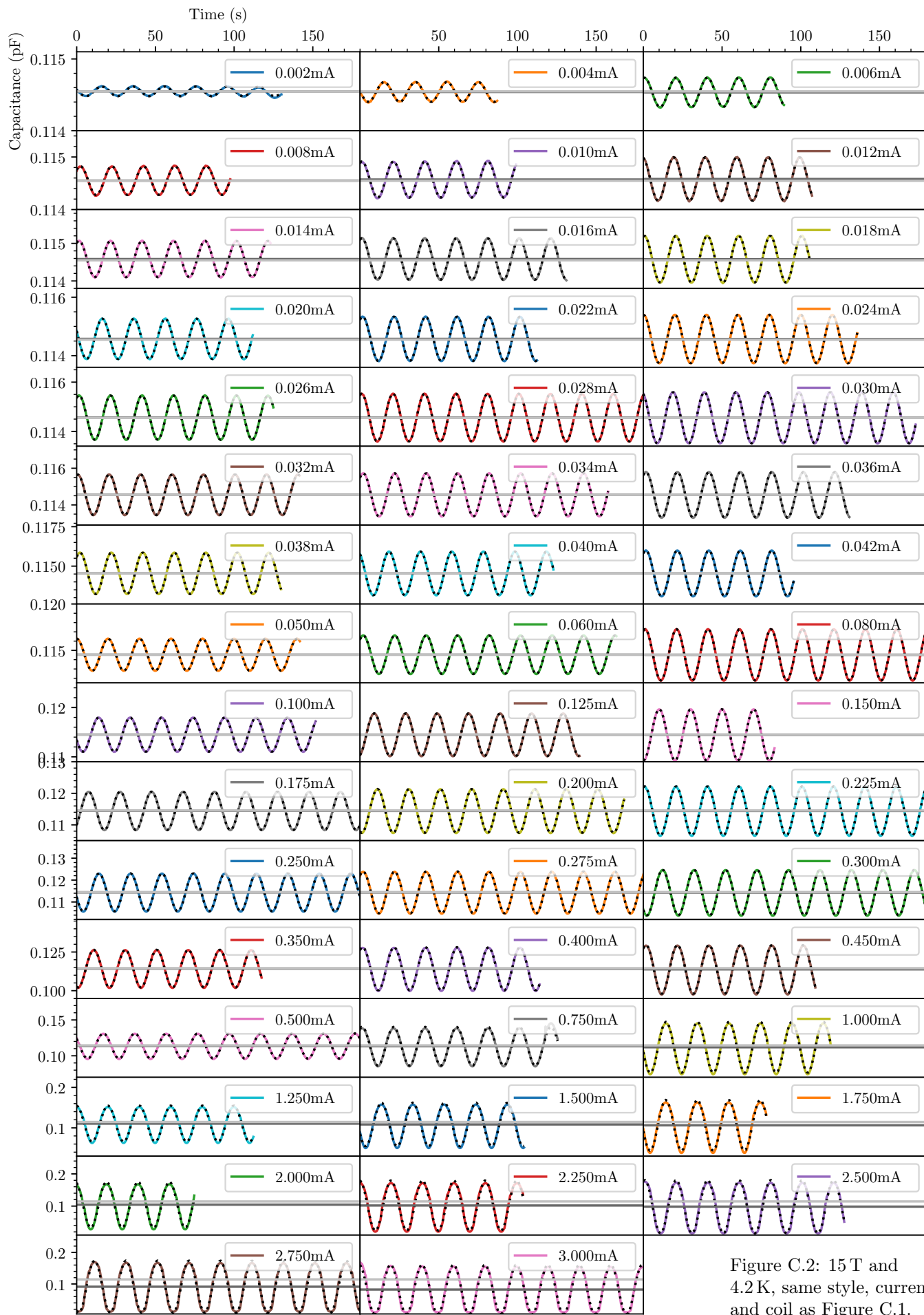


Figure C.2: 15 T and 4.2 K, same style, current and coil as Figure C.1.

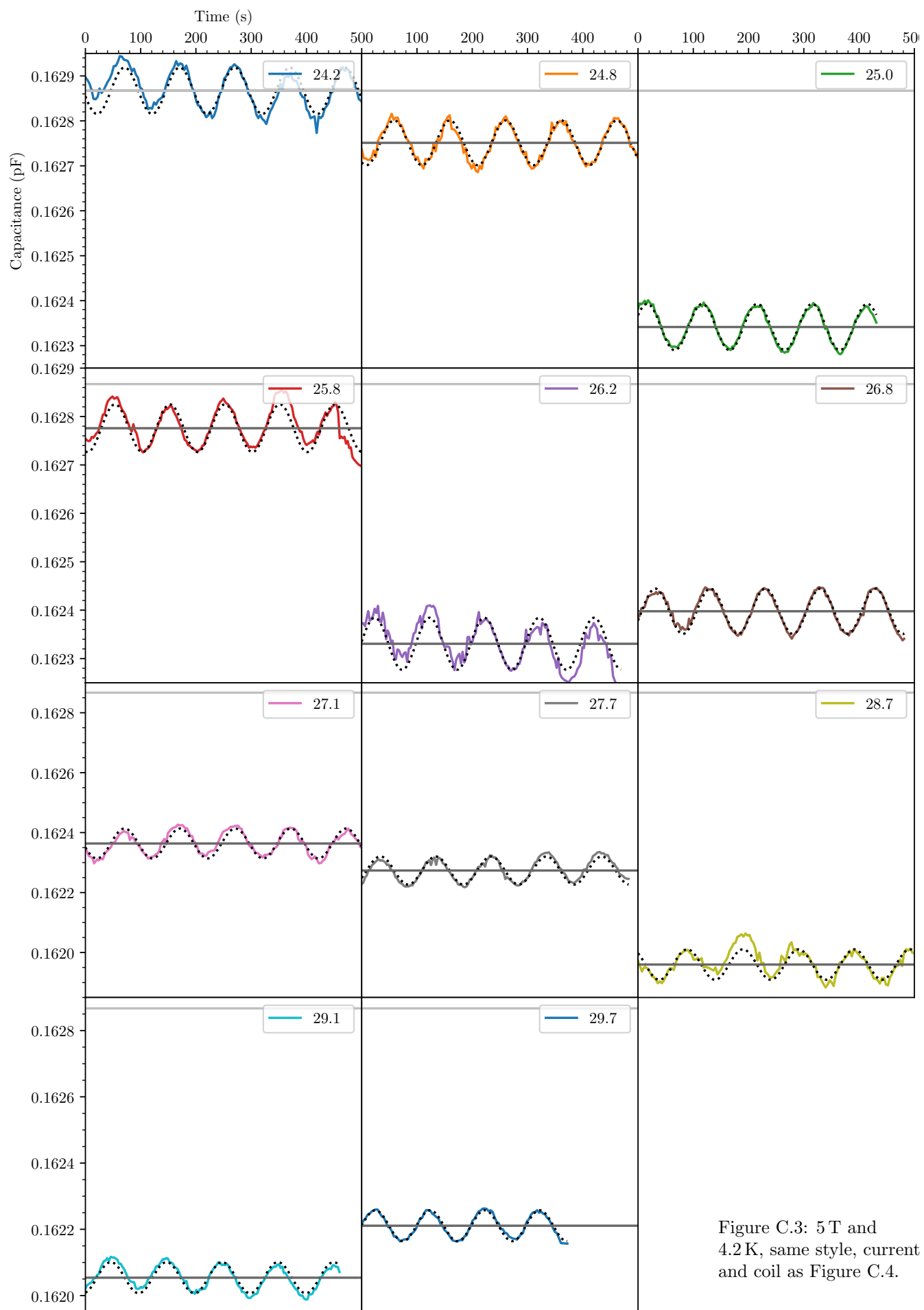


Figure C.3: 5 T and 4.2 K, same style, current and coil as Figure C.4.

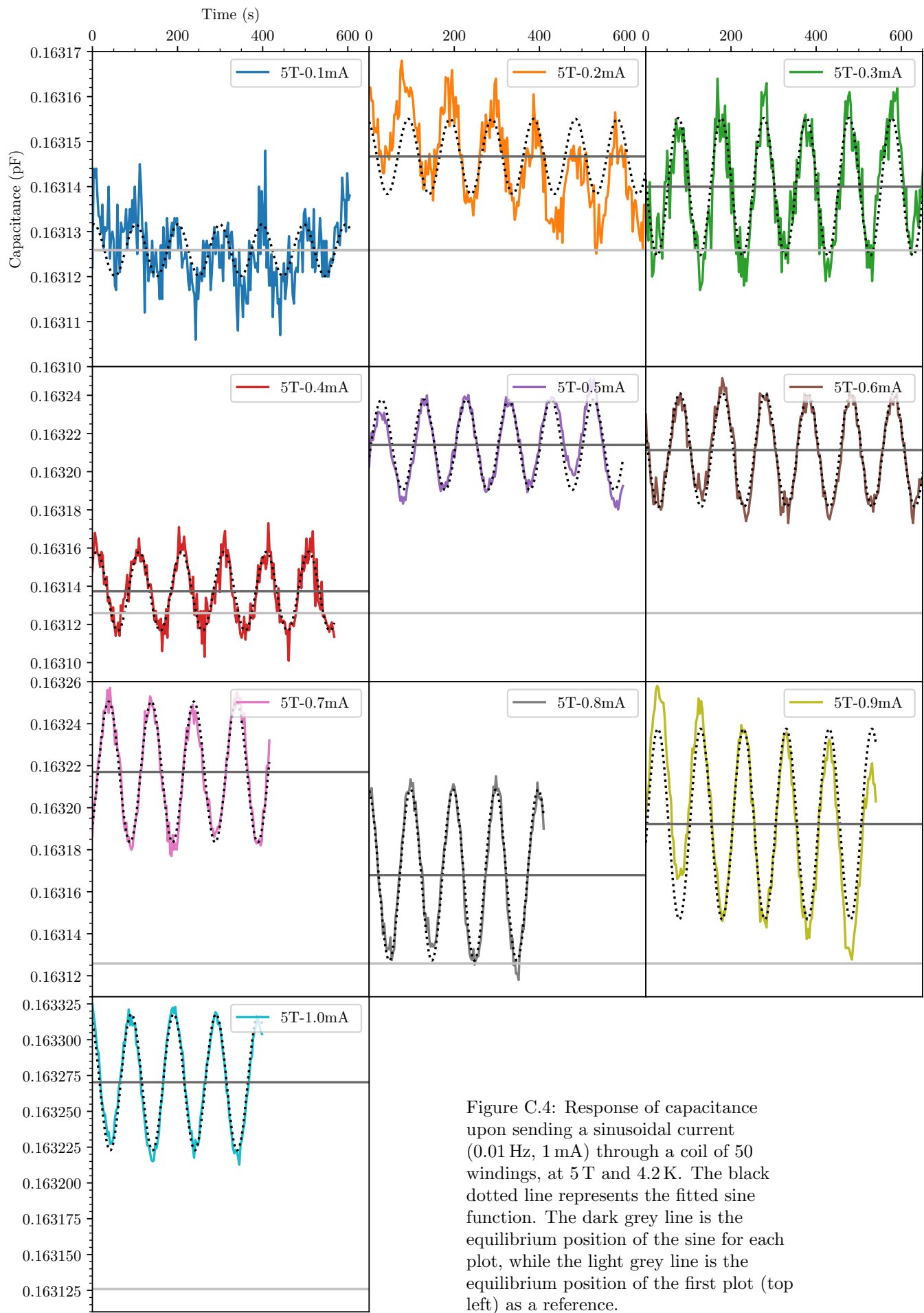


Figure C.4: Response of capacitance upon sending a sinusoidal current (0.01 Hz, 1 mA) through a coil of 50 windings, at 5 T and 4.2 K. The black dotted line represents the fitted sine function. The dark grey line is the equilibrium position of the sine for each plot, while the light grey line is the equilibrium position of the first plot (top left) as a reference.